e-photosynthesis: a comprehensive dynamic mechanistic model of C3 photosynthesis: from light capture to sucrose synthesis

XIN-GUANG ZHU[1,2,3], YU WANG[2], DONALD R. ORT[3,4] & STEPHEN P. LONG[3]

[1]*State Key Laboratory of Hybrid Rice and* [2]*CAS Key Laboratory for Computational Biology, CAS-MPG Partner Institute for Computational Biology, Shanghai Institutes for Biological Sciences, CAS, Shanghai 200031, China, and* [3]*Institute of Genomic Biology and Department of Plant Biology, University of Illinois at Urbana Champaign and* [4]*Global Change and Photosynthesis Research Unit, USDA/ARS, 1406 Institute of Genomic Biology, Urbana, IL 61801, USA*

ABSTRACT

Photosynthesis is arguably the most researched of all plant processes. A dynamic model of leaf photosynthesis that includes each discrete process from light capture to carbohydrate synthesis, *e*-photosynthesis, is described. It was developed by linking and extending our previous models of photosystem II (PSII) energy transfer and photosynthetic C3 carbon metabolism to include electron transfer processes around photosystem I (PSI), ion transfer between the lumen and stroma, ATP synthesis and NADP reduction to provide a complete representation. Different regulatory processes linking the light and dark reactions are also included: Rubisco activation via Rubisco activase, pH and xanthophyll cycle-dependent non-photochemical quenching mechanisms, as well as the regulation of enzyme activities via the ferredoxin-theoredoxin system. Although many further feedback and feedforward controls undoubtedly exist, it is shown that *e*-photosynthesis effectively mimics the typical kinetics of leaf CO₂ uptake, O₂ evolution, chlorophyll fluorescence emission, lumen and stromal pH, and membrane potential following perturbations in light, [CO₂] and [O₂] observed in intact C3 leaves. The model provides a framework for guiding engineering of improved photosynthetic efficiency, for evaluating multiple non-invasive measures used in emerging phenomics facilities, and for quantitative assessment of strengths and weaknesses within the understanding of photosynthesis as an integrated process.

Key-words: ATPase; chlorophyll fluorescence quenching; cytochrome b₆f; phenomics; photoprotection; photorespiration; Rubisco activase; Rubisco; systems biology; thioredoxin.

INTRODUCTION

Farquhar, Von Caemmerer & Berry (1980) developed a steady-state mechanistic model of C₃ leaf photosynthetic carbon assimilation rate (A), which was subsequently modified (Harley & Sharkey 1991). This model reasons that A, under any given set of conditions, will be limited by the slowest three processes: (1) the maximum rate of ribulose bisphosphate carboxylase/oxygenase (Rubisco) catalysed ribulose 1,5-bisphosphate (RuBP) carboxylation (Rubisco limited); (2) the regeneration of RuBP controlled by electron transport rate or enzymes in the C3 cycle other than Rubisco (RuBP regeneration limited); and (3) the regeneration of RuBP controlled by the rate of triose-phosphate utilization (TPU limited). This model has been widely validated in predicting steady-state A under different environmental conditions (Beadle & Long 1985; Harley & Sharkey 1991; Harley *et al.* 1992; von Caemmerer 2000). However, photosynthesis is rarely at steady state in the natural environment due to fluctuating conditions of light, temperature, vapour pressure deficit, and other conditions, as well as feedbacks within the leaf. Furthermore, without explicit representation of each enzyme in photosynthesis, the Farquhar *et al.* (1980) model cannot alone be used to predict the impact of manipulating different genes and their protein products on A.

In terms of total global food production, wheat, rice and soybean are the major C3 crops. It has become increasingly recognized that breeding of these crops has reached a point where further improvement of the potential yield is limited by photosynthetic capacity (Furbank *et al.* 2009; Long & Ort 2010; Zhu, Long & Ort 2010; Parry *et al.* 2011). The goal of identifying molecular targets to improve photosynthetic efficiency under field conditions as a means to improve crop yield would be significantly advanced by a comprehensive dynamic model of photosynthesis that includes as many photosynthesis-related reactions as possible (Zhu *et al.* 2010). The control of system flux in photosynthesis, which involves a complex series of interlinked biophysical and biochemical reactions, shifts among different reactions under different environmental conditions. Highly mechanistic, well-validated mathematical models of photosynthesis offer a practical means to select and prioritize among the multitude of potential permutations of targets for modification in engineering improved photosynthetic performance. This goal that has gained added importance as means other than photosynthesis in improving the potential yield of crop germ plasm are nearly exhausted (Long *et al.* 2006; Zhu, Long & Ort 2008; Zhu *et al.* 2010).

A comprehensive model of photosynthesis should include not only the individual steps, but also the major regulatory mechanisms affecting these steps, for example, the lumenal pH (Kramer, Sacksteder & Cruz 1999), the redox state of the plastoquinone pool in the thylakoid membrane (Stirbet,

Strasser & Strasser 1998), stromal pH (Martin, Scheibe & Schnarrenberger 2000), the redox state of thioredoxin (Schurmann & Jacquot 2000), its target enzymes (Hutchison *et al.* 2000) and the concentrations of key ions in the stroma and thylakoid lumen (Martin *et al.* 2000). Such an intricate model requires considerable computational power and advanced numerical algorithms to solve the resulting system of differential equations. This is especially so since the component reactions act on time scales that vary by orders of magnitude resulting in a stiff system of differential equations with respect to numerical integration (Zhu, De Sturler & Long 2007; Zhu *et al.* 2005). Algorithms have now been developed to deal with these stiff systems. These include variable order solvers that significantly improve computational efficiency (Shampine & Reichelt 1997; Shampine, Reichelt & Kierzenka 1999) and make it now possible to build a more complete model of photosynthesis than had been possible previously. The coalescence of an advanced knowledge about photosynthetic mechanisms, expanded computational power and efficient numerical integration algorithms provided this new opportunity to develop *e*-photosynthesis, the model presented here, as a quantitative framework for assessing knowledge and properties of the overall system.

Historically, mathematical models of photosynthesis with different levels of detail have been developed and used to test different hypotheses (Hahn 1984; Laisk & Walker 1986; Woodrow 1986; Pettersson & Ryde-Pettersson 1988; Laisk & Walker 1989; Laisk *et al.* 1989b; Gross, Kirschbaum & Pearcy 1991; Hahn 1991; Rovers & Giersch 1995; Laisk *et al.* 1997; Pearcy, Gross & He 1997; Laisk & Edwards 2000; Poolman, Fell & Thomas 2000; Laisk, Eichelmann & Oja 2006). For example, mathematical models of carbon metabolism have been developed to study the control of photosynthetic CO_2 flux within the C3 cycle in isolation (Woodrow 1986; Poolman *et al.* 2000; Poolman, Assmus & Fell 2004), photosynthetic oscillations (Laisk *et al.* 1989a; Walker 1992) or the optimization of resource use investment between the enzymes of carbon metabolism at light saturation (Zhu *et al.* 2007). Because these models were usually developed to test particular hypotheses, each model simplified processes that were not critical for testing the target hypothesis. Laisk *et al.* (2006) developed a detailed C3 photosynthesis model including both carbon metabolism and the 'light reactions', showing the growing interest in simulating the whole photosynthetic process, rather than individual parts of the system. Here we present a significantly more complete model of photosynthesis by extending these previous models, particularly the model of fluorescence induction (Zhu *et al.* 2005) and the model of carbon metabolism (Zhu *et al.* 2007). Our model presented here, *e*-photosynthesis, includes (1) the detailed reactions in the C3 cycle, sucrose synthesis, starch synthesis and photorespiration; (2) the detailed reactions associated with light absorption, excitation energy transfer, charge separation, electron transfer around both photosystem II (PSII) and photosystem I (PSI), ion transfer between the lumen and stroma, as well as ATP and NADPH synthesis; (3) the major regulatory processes involved in photosynthesis, including Rubisco activation via Rubisco activase, non-photochemical quenching via luminal pH and the xanthophyll cycle, and the regulation of enzyme activities via the ferredoxin thioredoxin system. This article (1) describes the structure, assumptions, rate equations, differential equations and parameters used in the *e*-photosynthesis model; (2) shows that *e*-photosynthesis provides qualitatively and quantitatively realistic simulations of *in vivo* leaf photosynthesis through a series of *in silico* experiments; (3) uses *e*-photosynthesis to analyse the potential mechanisms underlying the classical chlorophyll fluorescence decay curve following induction of photosynthesis upon a dark to light transition.

MODEL DESCRIPTION

The parameters and assumptions for the reactions from water splitting to PQH_2 formation are given in Zhu *et al.* (2005) and for carbon metabolism in Zhu *et al.* (2007), and are listed in Supporting Information Appendix S1. The following explains the assumptions for the additional discrete processes added here to develop *e*-photosynthesis.

Model structure and assumptions for reactions associated with the thylakoid membrane

1 Reduced plastoquinone (PQH_2) is oxidized through the cytochrome b_6f complex (cyt b_6f), which consists of a c-type haem (cytochrome f), two b-type haems, an iron sulphur protein (ISP), a haem c_n (formerly known as haem X) and single molecules of chlorophyll *a* and carotenoid (Fig. 1). The mitochondrial and bacterial cyt bc_1 complexes (cyt bc_1) are in the same cyt bc family as cyt b_6f and all are regarded to operate using the same modified Q cycle mechanism (Berry *et al.* 2000). Therefore, the much more prevalent kinetic parameters of reduction and oxidation in the cyt bc_1 complex were used in our model of electron transfer to describe the modified Q cycle around the cyt b_6f complex. Cyt b_6 in the cyt b_6f complex is the counterpart of cyt b in cyt bc_1; cyt f in cyt b_6f complex is the counterpart of cyt c_1 in cyt bc_1 (Berry *et al.* 2000). However, the cyt bc_1 complex lacks the chlorophyll and carotenoid molecules and cyt c_n of cyt b_6f. But since their function is unknown, they could not be included in the current version of the model.

2 There are three confirmed catalytic sites on cyt b_6f for binding external substrates: the plastoquinol (PQH_2) binding site (Q_p site) and the plastocyanin (PC) binding site on the lumen (p) side, and the plastoquinone (PQ) binding site on the stromal (n) side of the thylakoid membrane (Q_n site). In addition to these three catalytic sites: there are two additional catalytic interfaces (at cyt f and cyt b_{6L}), which are involved in the oxidation of PQH_2 at the Q_p site (Berry *et al.* 2000).

3 According to the modified Q cycle, the oxidation of PQH_2 at the Q_p site begins by formation of the substrate complex, $ISP_{(ox)}.PQH_2$ (Hong *et al.* 1999; Berry *et al.* 2000; Crofts *et al.* 2000). Oxidation of $ISP_{(ox)}.PQH_2$ is assumed here to occur in two steps. Firstly, one electron is
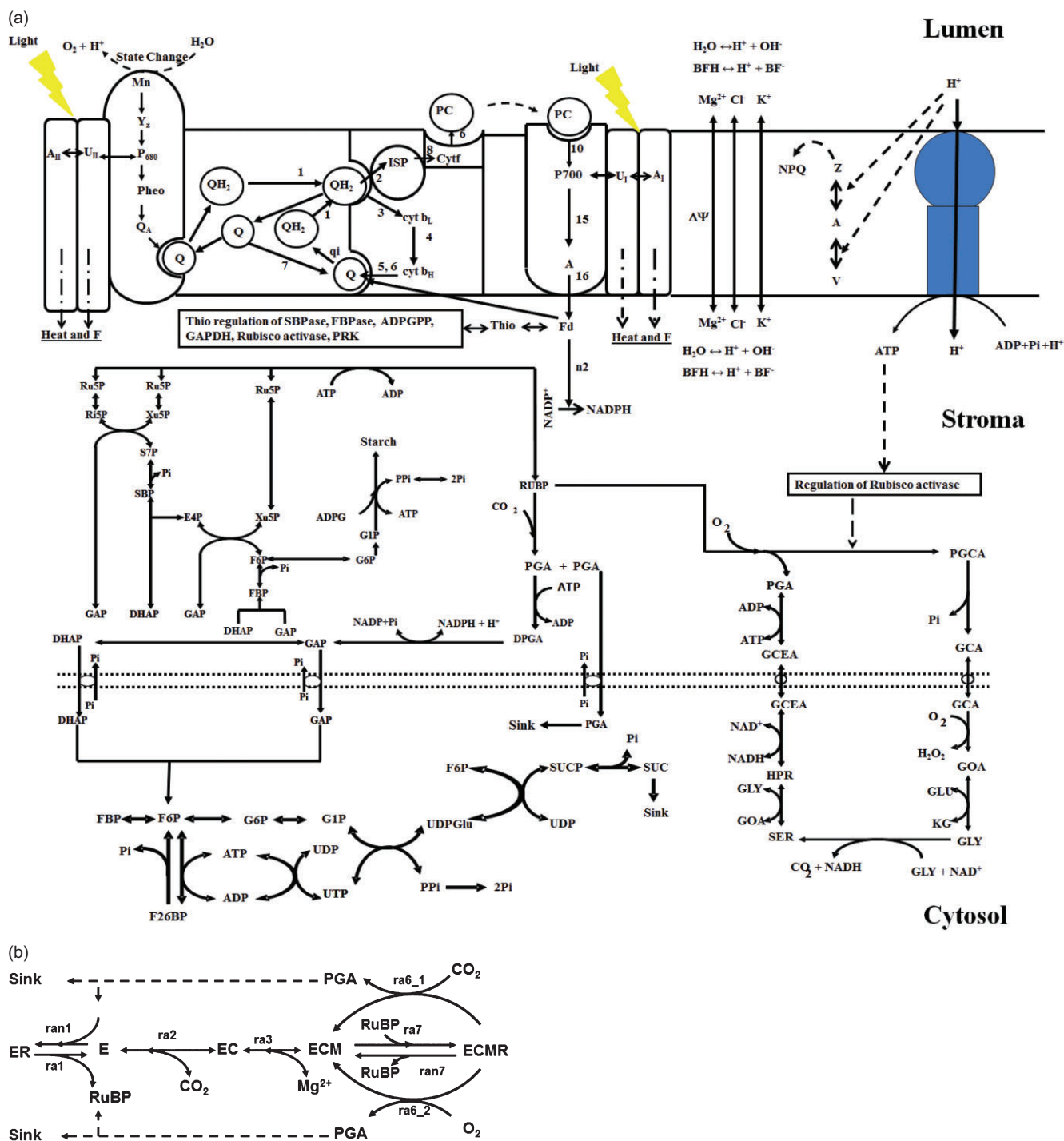
Figure 1. (a) Diagrammatic representation of the individual processes included in *e*-photosynthesis. The numbers by each reaction are used as subscripts in the rate equation for each reaction. The numbers for reactions in the carbon metabolism follow Zhu *et al.* (2007) (b) Details of the steps represented in activation/deactivation of Rubisco (E) associated with Rubisco activase. Definitions of abbreviations are given in Tables 1.1 and 1.2 in Supporting Information Appendix S1.

transferred to a high-potential chain followed by the other to a low-potential chain, in the so-called bifurcated reaction (Hong *et al.* 1999). The high-potential chain in chloroplasts consists of ISP, cyt f and plastocyanin (PC). PC is a water-soluble Cu-containing protein, which acts as a mobile electron carrier, oxidizing cyt f on the lumen side

and shuttling the electron to the oxidized primary donor of PSI (P_{700}; Cramer *et al.* 1996; Berry *et al.* 2000). The chloroplast low-potential chain consists of cyt b_{6L} and cyt b_{6H}, which form the electron transfer pathway across the membrane from the Q_p site to the Q_n site to reduce PQ (Cramer *et al.* 1996; Berry *et al.* 2000).

4 Reduced ISP coexists at equilibrium in either the proto-
   nated (ISPH) or the deprotonated state (ISP⁻) with a pK_a
   of 7.6 (Ugulava & Crofts 1998; Crofts *et al.* 2000). It was
   assumed in our model that ISPH and ISP⁻ donate elec-
   trons to cyt f with equal probability and are therefore
   represented by identical rate equations.

5 PQ in the Q_n site of cyt b_6f is assumed to become fully
   reduced (PQ^{2-}) after receiving two electrons from the
   low-potential chain. The rate of protonation of PQ^{2-} has
   been shown to vary with pH, and the empirically derived
   relationship is used to capture this effect (Taly *et al.* 2003).

6 It is assumed that the PQH_2 formed at the Q_n site is
   readily available for formation of $PQH_2.ISP$ at the Q_p site
   with oxidized ISP.

7 PSI has both core and peripheral (LHCI) antenna. Oxi-
   dized P_{700} oxidizes PC, and in turn reduces a chlorophyll a
   molecule, A_0. The other intermediate electron transfer
   steps between ferredoxin and A_0 are ignored (Fig. 1).

8 In *e*-photosynthesis, the proton motive force (*pmf*) for
   ATP synthesis incorporates both a chemical and an elec-
   trical potential across the thylakoid membrane. The
   observed activation behaviour of ATP synthase suggests a
   minimum *pmf*, which varies depending on the
   thioredoxin-regulated redox state of a pair of cysteines in
   the γ-subunit of ATP synthase (Ort *et al.* 1990; Ort &
   Oxborough 1992). It is assumed that translocation of 4.67
   protons from lumen to stroma is needed for formation of
   1 ATP (Vollmar *et al.* 2009).

9 In this model, the transport of Mg^{2+}, K^+ and Cl^- across the
   thylakoid membrane is simulated explicitly and used to
   calculate the electrical potential across the thylakoid
   membrane. The fluxes of ions between the cytoplasm and
   stroma are assumed not to cause significant changes in
   electrical potential across the thylakoid membrane
   (Thaler, Simonis & Schonknecht 1992). Although these
   ions are cofactors or effectors of some enzymes of carbon
   metabolism, these effects are not included in the current
   model, with the exception of the effect of $[Mg^{2+}]$ on
   Rubisco activation, as described later.

10 Although multiple buffer species are present in each
   plastid compartment, it is assumed that buffering in a
   compartment can be represented by a single empirical
   equation, which captures the observed buffering of pH
   (Junge *et al.* 1979; Junge & McLaughlin 1987).

11 *e*-Photosynthesis incorporates the regulation of light uti-
   lization through non-photochemical quenching (NPQ)
   following the mechanism of NPQ suggested by Crofts &
   Yerkes (1994). This assumes that NPQ occurs in one of
   the minor chlorophyll protein complexes associated with,
   rather than within, the reaction centre of PSII. Acidifica-
   tion of the lumen during illumination leads to protona-
   tion of acidic ligands (e.g. glutamine) and changes the
   ligating properties (Crofts & Yerkes 1994), which in turn
   leads to increased NPQ in the form of heat dissipation
   (Horton, Ruban & Walters 1996; Niyogi 1999).

12 It is assumed that the ratio of [PSII unit]:[cyt b_6f]:[PSI
   unit]:[PC]:[ferredoxin] = 1:1:1:1:1 and that the amount of
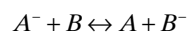   cyt b_6f on a leaf area basis is 1 μmol m^{-2}, as in the model

of fluorescence induction (Zhu *et al.* 2005). The volumes
of the lumen and stroma were calculated from structural
measurements. Specifically, a leaf is assumed to be 0.5 mm
thick; 58.5% of the leaf volume is assumed to be meso-
phyll and 9.5% of the mesophyll cell is assumed to be
chloroplast stroma (Winter, Robinson & Heldt 1994). The
ratio of stroma to lumen volume varies depending on
plant species, developmental stages and growth condi-
tions (Pyke 1999). In this model, the ratio of the lumen
volume to stroma volume is taken to be 1:1. Based on
these assumptions, the volumes of stroma and lumen for
1 m^2 leaf area are $0.5 \times 10^{-3} \times 58.5\% \times 9.5\%$ m^{-3} = 27 mL.
Thus, there are 27 mL stroma and 27 mL lumen for 1 m^2
of leaf area.

Rate equations for reactions associated with membrane

The rate equations used in describing rate of electron trans-
fer were derived following the assumptions and conditions
described above.

The generalized rate equations

Unless stated otherwise, rate equations use generalized mass
action kinetics. Where the reaction sequence is uncertain or
random, the approach of convenience kinetics is used as
described by Liebermeister & Klipp (2006). For electron
transport, this approach is used to formulate generalized rate
equations of the form A^- to B modified from Laisk & Walker
(1989):

$$A^- + B \leftrightarrow A + B^-$$

$$v = V_{max} \left(\frac{[A^-]}{[A^-]+[A]} \frac{[B]}{[B^-]+[B]} - \frac{[A]}{[A^-]+[A]} \frac{[B^-]}{([B^-]+[B])K_E} \right)$$
(1)

$$V_{max} = k_{AB} \cdot \min\{[A^- + A],[B^- + B]\}$$
(2)

$$k_{AB} = \frac{\ln 2}{t_{1/2}}$$
(3)

$$\Delta E = E_B - E_A$$
(4)

$$\Delta G = -nF\Delta E$$
(5)

$$K_E = \exp(-\Delta G/RT)$$
(6)

where V_{max} is the maximum rate of electron transport from
A^- to B. k_{AB} is the rate constant of this electron transfer
reaction, which was calculated from the half-time ($t_{1/2}$) of the
reaction using Eqn 3 (Chang 2000). The change of the free
energy of the electron transfer reaction, ΔG, was calculated
based on the product of the difference between the midpoint
potentials of the electron acceptor (E_B) and the electron

donor (E_A), the number of electrons transferred per molecule of product (n) and the Faraday constant (F; Eqns 4, 5). The ΔG is further used to derive the equilibrium constant of the reaction, K_E (Eqn 6).

## Rate equations for individual steps

As stated in the assumptions, the reactions of cyt bc_1(Crofts 1985; Berry *et al*. 2000) are used to represent cyt b_6f taking advantage of their functional similarity and the abundance of kinetic parameters for cyt bc1.

1 $ISP_{ox} + PQH_2 \rightarrow ISP_{ox}.PQH_2$
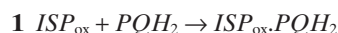
$$v_{bf1} = V_{max1} \frac{[ISP_{ox}]}{([ISP_{(ox)}]+[ISPH_{(red)}])} \frac{[PQH_2]}{([PQ]+[PQH_2]+[PQH])} \tag{7}$$

Where V_{max1} is the maximum rate of the reaction and is assumed to be limited by the rate of PQH_2 diffusion within thylakoid membrane.

PQH_2 oxidation shows a strong pH dependency, which is due to the dependency of the deprotonation of oxidized iron-sulphur protein (ISPH$^+$) on pH (Hong *et al*. 1999). Deprotonation of ISPH$^+$ increases the amount of ISP_{ox}, and therefore, the rate of formation of $ISP_{ox}.QH_2$ (Crofts *et al*. 2000). The pK_a for ISPH$^+$ deprotonation is 7.6 for cyt bc$_1$ (Ugulava & Crofts 1998; Crofts *et al*. 2000). The ISP_{ox} concentration is calculated as
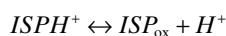
$ISPH^+ \leftrightarrow ISP_{ox} + H^+$

Since $\quad pK = -\log \frac{[ISP_{ox}][H^+]}{[ISPH^+]}$, which can be rearranged

to as

$$[ISP_{ox}] = \frac{[ISP_{oxt}]}{1+\frac{[H^+]}{[10^{-pK}]}}; \tag{8}$$

where [H^+] represents the lumenal proton concentration and [ISP_{oxt}] represents the sum of [$ISPH^+$] and [ISP_{ox}].

**2** $ISP_{ox}.PQH_2 \rightarrow PQH + ISPH_{red}$
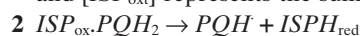
This is the first electron transfer step in PQH_2 oxidation and has a high activation barrier due to a coupled proton and electron transfer in this process (Hong & Xu 1999; Crofts *et al*. 2000). The rate equation for this reaction is assumed to be

$$v_{bf2} = k_{bf2}[ISP_{ox} \cdot PQH_2]f_{pH} \tag{9}$$

where k_{bf2} is the rate constant of this reaction and f_{pH} incorporates the effect of lumen pH on this reaction. The effect of luminal pH is incorporated by assuming that a hypothetical residue with a pK_a of 5.5 controls the rate of PQH_2 oxidation. Further, this reaction reaches its maximum rate at pH 8 and the rate then declines proportionally with the degree of protonation of the hypothetical residue with further increase in pH (Witt 1979; Nishio & Whitmarsh 1993; Cruz *et al*. 2001). The maximum rate of the electron transfer from PQH_2 to ISP_{ox} was assumed to be 150 mol s^{-1} (Crofts *et al*. 2000). The equation of f_{pH} is given in Supporting Information Appendix S3 section 1.1.

3 $PQH + cyt\ b_L \rightarrow PQ + H^+ + cyt\ b_L^-$
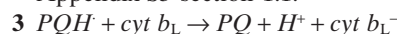
No direct measurement of the rate of this electron transfer reaction is available (Crofts *et al*. 2000). We used a value of 5×10^7 s^{-1} based on theoretical estimates (Hong *et al*. 1999). It is further assumed that lumenal pH regulates this step in a similar manner as electron transfer from PQH_2 to ISP and this is represented by f_{pH} (Cruz *et al*. 2001). In the following six electron transfer reactions, the generalized rate constant k_{AB} of Eqn 2 is replaced by a specific rate constant for the assumed irreversible forward reaction. Since these equations determine the rate of electron transfer of the bound electron donor, this rate will be affected by the oxidation state of the acceptor, which is represented by the ratio of oxidized to total acceptor. Therefore, the rate equation for this reaction is

$$v_{bf3} = k_{bf3}f_{pH}[PQH]\frac{[Cyt\ b_L]}{[Cyt\ b_T]} \tag{10}$$

Where k_{bf3} is the rate constants of this reaction.

**4** $ISPH_{(red)} + cyt\ f \rightarrow ISPH^+_{(ox)} + cyt\ f^-$
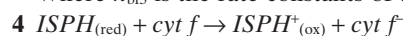
Generalized rate equations (Eqns 1–6) are used to calculate the rate of this reaction. The half-time of this reaction ($t_{1/2}$) in Eqn 3 is assumed to be 3 ms (Fernandez-Velasco *et al*. 2001). It is also assumed that the midpoint potentials (E) of Eqn 4 is 0.310 V for ISP (Hong *et al*. 1999) and 0.270 V for *cyt f* (Chen 1989).

5 $Cyt\ b_L^- + Cyt\ b_H \rightarrow Cyt\ b_L + Cyt\ b_H^-$
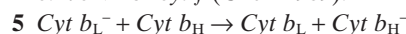
The maximum rate constant for the electron transfer from *cyt* b_L^- to *cyt* b_H is assumed to be the modal value of the theoretically calculated rate constant from QH to *cyt* b_L, that is, 5.7×10^7 s^{-1} (Hong *et al*. 1999; Crofts *et al*. 2000). As an approximation, we assume that b_H/b_H^{-1} and b_L/b_L^{-1} are isopotential, and therefore, midpoint potentials are not included in the calculation:

$$v_{bf4} = k_{bf4}[Cyt\ b_L^-]\frac{[Cyt\ b_H]}{[Cyt\ b_T]} \tag{11}$$

6 $Cyt\ b_H^- + PQ \rightarrow PQ^- + Cyt\ b_H$ and $Cyt\ b_H^- + PQ^- \rightarrow PQ^{2-} + Cyt\ b_H$
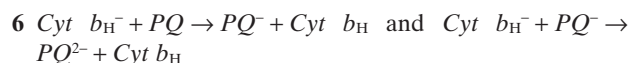
Similar to Eqns 10 and 11, the maximum rate constant for these two electron transfer steps is assumed to be 5×10^7 s^{-1} (Hong *et al*. 1999) and the rate equations used for these reaction are

$$v_{bf5} = k_{bf5}[Cyt\ b_H^-]\frac{[PQ_{nb}]}{[Cyt\ b_T]} \tag{12}$$

$$v_{bf6} = k_{bf6}[Cyt\ b_H^-]\frac{[PQ^-]}{[Cyt\ b_T]} \tag{13}$$

Where [PQ_{nb}] represents the concentration of plastoquinone bound to the Q_n site of *cyt b$_6$f*. The concentration of the bound plastoquinone is calculated based on the availability of empty plastoquinone binding sites and the concentration of available free plastoquinone in thylakoid membrane. [Q^-] is the concentration of unprotonated plastosemiquinone.

7 Binding of free plastoquinone (*PQ*) to Q_n site of *cyt b$_6$f*

This model assumes that the rate of *PQ* binding to the Q_n site depends on the concentrations of both free plastoquinone ([PQ]) and empty Q_n sites ([Q_{se}]), the rate equation for this reaction is formulated as

$$v_{bf7} = k_{bf7}[Cyt\ b_T]\frac{[Q_{se}]\ [PQ]}{[Q_{sT}]\ [PQ_T]} \tag{14}$$

where [Q_{sT}] represents the total concentration of plastoquinone-binding sites in *cyt b$_6$f* and [PQ] represents the concentration of free plastoquinone. [PQ_T] represents the total concentration of bound and unbounded plastoquinone, both oxidized and reduced. This reaction is rapid compared to *PQH$_2$* oxidation at the Q_p site (i.e. $ISP_{ox}.PQH_2 \rightarrow PQH\cdot + ISPH_{red}$), which has a rate constant of 150 s^{-1} (Crofts *et al.* 2000). Therefore, as a simplification, we assumed k_{bf7} to be 10^4 s^{-1}.

8 Electron transfer from *cyt b$_6$f* to *PC*

As stated above (see the section *Model structure and assumptions for reactions associated with membrane*), we assume that *cyt f* and plastocyanin equal the known reactions of *cyt c$_1$* and *cyt c$_2$* of the *cyt bc$_1$* complex:

$$cyt\ f^- + PC^+ \leftrightarrow cyt\ f + PC$$
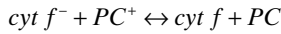
The general rate equations (Eqns 1–6) were used to calculate the rate of this reaction. The E_m for *PC* is 0.350 V and 0.270 V for *cyt f* (Chen 1989). The V_{max} for this reaction is 8.3×10^6 mol L^{-1} s^{-1} (Chen 1989).

9 Electron transfer from plastocyanin to P_{700}

The rate equation for this reaction is assumed as

$$v_{bf10} = k_{bf10}\left(\frac{[PC][P_{700}^+]}{[P_{700T}]} - \frac{[PC^+][P_{700}]}{[P_{700T}]K_{10}}\right) \tag{15}$$

where [P_{700T}] represents the total concentration of P_{700} and the k_{bf10} is calculated based on a $t_{1/2}$ of 4 μs (Bowyer, Tierney & Crofts 1979a,b) and K_{10} is the equilibrium constant of this reaction.

10 Plastoquinone protonation

Formation of *PQH$_2$* from *PQ^{2-}* was assumed to occur with a V_{max} as 5.7×10^7 s^{-1}, based on the theoretical calculation of the rate of electron transfer from *PQH$\cdot$* to *cyt b$_L$* (Hong *et al.* 1999). The concentration of the reduced plastoquinol at the Q_n site ([PQ^{2-}]) and the stromal pH influence the rate of plastoquinone protonation. This is represented as

$$v_{qi} = 2k_{qi}[PQ^{2-}]f_{Ph2} \tag{16}$$

where k_{qi} is the rate constant for this reaction, f_{Ph2} incorporates the effects of pH on this reaction, which is derived

from empirical data for the protonation of *PQ$_B^{2-}$* (Taly *et al.* 2003), which we assume to behave similarly to *PQ^{2-}* bound at the Q_n site.

11 ATP synthesis

The rate of *ATP* synthesis was assumed to follow Michaelis–Menten kinetics (Eqn 17). The equilibrium constant for *ATP* synthesis is calculated based on the Gibbs free energy of the reaction (Eqn 18), which is in turn determined by the proton motive force including both $\Delta\Psi$ and ΔpH components and the standard Gibbs free energy for this reaction (ΔG°). $\Delta\Psi$ is calculated using Eqn 22 described later. The contribution of ΔpH to the Gibbs free energy is represented by $0.592HPR(\ln[H_{fl}]/[H_{fs}])$ where *HPR* is the proton/*ATP* ratio, that is, the number of proton translocation needed for formation of 1 ATP. In this model, *HPR* is assumed to be 4.67 (Vollmar *et al.* 2009).

$$v_{bf1} = \frac{V_{bf1max}\left([ADP][Pi] - \dfrac{[ATP]}{kE}\right)}{(K_{mADP}K_{mP})\left(1 + \dfrac{[ADP]}{K_{mADP}} + \dfrac{[Pi]}{K_{mP}} + \dfrac{[ATP]}{K_{mATP}} + \dfrac{[ADP][Pi]}{K_{mADP}K_{mP}}\right)} \tag{17}$$

$$kE = e^{(-\Delta G/RT)} \tag{18}$$

$$\Delta G = \Delta G^\circ + 0.592\ HPR \ln\left(\frac{[H_{fl}]}{[H_{fs}]}\right) + HPR\ \Delta\Psi \tag{19}$$

where V_{bf1max} is the maximum rate of this reaction; H_{fl} and H_{fs} represent the concentrations of proton in the lumen and stroma, respectively, which were calculated using standard buffering equations (Eqns 24, 25). K_{mADP}, K_{mATP}, K_{mP} represent the Michaelis–Menten constants for ADP, ATP and Pi.

12 Ion movement through the thylakoid membrane

In order to calculate $\Delta\Psi$, the movements of ions across thylakoid membrane must be simulated. These are driven by transmembrane electrical and concentration differences, which is described by the Nernst–Plank equation (Eqn 20). Equation 21 is the solution of this equation used in *e*-photosynthesis to calculate ion flux (Bockris & Reddy 1970). Here, the fluxes of ions across the thylakoid membrane depend on $\Delta\Psi$, the lumenal concentration of the ion (I_i), the stromal concentration of the ion (I_e) and the permeability constant (P) for the ion. The fluxes of K$^+$, Mg^{2+} and Cl$^-$ were calculated individually with this equation. The electrical potential across the thylakoid membrane, $\Delta\Psi$, was calculated based on the difference in charges between the stroma (Q_c) and lumen and electrical capacitance (C) of the thylakoid membrane (Eqns 22 and 23). The net charge in the thylakoid lumen is equal and opposite to that in the stroma; therefore, the difference in charge between stroma and lumen is equal to twice the net charge in stroma (Eqn 22). The ratio of stroma volume per unit thylakoid membrane area follows (Flores, Graan & Ort 1983; Cruz *et al.* 2001). As a

simplification, we assumed that the net charge in stroma and lumen is zero for dark-adapted leaves; therefore, the net charge across thylakoid membrane as a result of ion transfer and proton translocation is equal to twice the net charge in the stroma or in the lumen (Eqns 22 and 23).

$$J = -\mu RT \frac{d[I]}{dx} - zF\mu \frac{d\Psi}{dx} \tag{20}$$

$$J = P \frac{zF\Delta\Psi}{RT} \cdot \frac{\left([I_i] - [I_e]e^{-\frac{zF\Delta\Psi}{RT}}\right)}{1 - e^{-\frac{zF\Delta\Psi}{RT}}} \tag{21}$$

$$\Delta\Psi = \frac{2Q_c}{C} \tag{22}$$

$$Q_c = F([K_s^+] + [H_s^+] + 2[Mg_s^{2+}] - [Cl_s^-] - [OH_s^-] - [BF_s^-]) \tag{23}$$

where, $[OH_s^-]$ and $[BF_s^-]$ are the concentrations of hydroxyl ions and the buffer species, respectively, in the stroma (s). Chloroplast $[Mg^{2+}]$ ranges from 2 to 18 mM, a significant amount of which is possibly bound to thylakoid membrane, LHC complexes and nucleotides (Barber 1976; Schroppelmeier & Kaiser 1988). K^+ and Na^+ are also major cations in the chloroplast (Schroppelmeier & Kaiser 1988). The permeability of Mg^{2+} and K^+ through thylakoid cation channels is similar (Pottosin & Schonknecht 1996). No report on the permeability to Na^{2+} is available currently. K^+ and Mg^{2+} are assumed to be the major cations, which can permeate through the thylakoid membrane and therefore are the only ones included in this model.

Cl^- was assumed in our model to be the only anion, which can permeate through the thylakoid membrane between the stroma and lumen. The cytoplasmic $[Cl^-]$ has been estimated to be 1 to 3 mM (Schroppelmeier & Kaiser 1988; Thaler *et al*. 1992). The permeability coefficient of Cl^- is assumed as 1.8×10^{-8} cm s^{-1} as used by Cruz *et al*. (2001). As a simplification, it was assumed that in a dark-adapted leaf, the resting membrane potential is zero and that the different ions have equal concentrations in the stroma and the lumen.

The membrane electrical capacitance (C in Eqn 22) is approximately 0.6-1 μF cm^{-2} (Vredenberg 1976; Junge *et al*. 1979) and the ratio of lumen volume to thylakoid membrane single surface area was assumed to be 0.8 nL cm^{-2} (Vredenberg 1976; Vredenberg & Bulychev 1976).

13 Calculation of pH in stroma and lumen

Four photosynthetic reactions influence the combined total concentration of protons and protonated buffer species in lumen ([H$^+$] + [BFH]), that is, water oxidation (v_{s3_s0} in appendix 2 of Zhu *et al*. 2005), the electron transfer from PQH$^-$ to cyt b$_L$ (Eqn 10), electron transfer from ISPH$^+$ to cyt f (v_{bf8} in section 1.1 of Supporting Information Appendix S1) and ATP synthesis (Eqn 17). Four related photosynthetic reactions influence([H$^+$] + [BFH]) in the stroma, that is, ATP synthesis (Eqn 17), proton uptake at the Q_n site of cytb$_6$f complex (Eqn 16), proton

uptake at the Q_B site of PSII (v_{qb} in section 1.1 of Supporting Information Appendix S1) and NADPH formation (Eqn 33a).

Considering that several distinct buffer species exist in the stroma and the lumen, the pH of the stroma and lumen were calculated based on the measured buffer capacities and the changes in [H$^+$ + BFH] for each compartment. The buffer capacity for a group of buffer species is derived from the equilibrium equation for each individual buffer species. For example, for the ith buffer species in this group, the equilibrium equation is

$$K_i = \frac{[H^+][BF_i^-]}{[BF_iH]} \tag{24}$$

where K_i is the dissociation constant for proton binding to buffering group BF_i^-; $[BF_i^-]$ and $[BFH]$ are the concentrations of the deprotonated and protonated ith buffer species. The range of pKa values of the many buffering groups results in a linear change in pH in proportion to translocation of protons (Junge *et al*. 1979; Junge & McLaughlin 1987). The buffering capacity (K_b) is therefore defined as

$$K_b = \frac{\Delta\left([H^+] + \sum_{i=1}^{n}[B_iH]\right)}{\Delta(pH)} \tag{25}$$

In this model, the buffer capacities for lumen and stroma were assumed to be 0.03 and 0.02 mol L^{-1} (pH unit)$^{-1}$, respectively (Oja *et al*. 1999; Cruz *et al*. 2001).

14 Excitation energy absorption and transfer, and electron transport reactions around PSI.

The excited states of chlorophylls in the two antenna systems (peripheral antenna A_{IP} and core antenna U_I, Fig. 1) have one of three fates: photochemistry, heat dissipation and fluorescence with rate equations as follows:

$$v_{IPC} = [A_{IP}]k_{AU} \tag{26}$$

$$v_{ICP} = [U_I]k_{UA} \tag{27}$$

$$v_f = ([A_{IP}] + [U_I])k_{f,ps1} \tag{28}$$

$$v_d = ([A_{IP}] + [U_I])k_d \tag{29}$$

where v_{IPC} represents the rate of excitation energy transfer from the peripheral antenna to the core antenna of PSI; v_{ICP} represents the rate of excitation energy transfer from the core antenna to the peripheral antenna of PSI; v_f represents the rate of fluorescence emission from antenna, which is essentially zero for PS1 due to P700 quenching. Therefore, $k_{f,ps1}$ is assumed to be zero. Finally, v_d represents the rate of heat dissipation from the antenna and k_{AU} and k_{UA} represent the rate constants of excitation transfer from A_{IP} to U_I, and from U_I to A_{IP}, respectively.

15 Primary charge separation at the PSI reaction centre
$P_{700e} + A_0 \leftrightarrow P_{700e}^+ + A_0$ where P_{700e} represents the excited
PSI reaction centre (P_{700}). As previously assumed for P_{680},
P_{700} is assumed always to be in equilibrium with the
excited chlorophylls in the core antenna. The proportion
of excited P_{700} chlorophylls is given as

$$[P_{700e}] = [U_I] \frac{([P_{700T}] - [P_{700}^+])}{120} \tag{30}$$

where 120 represents the number of chlorophylls in the
core antenna of PSI including P_{700} (Horton *et al.* 1996;
Chitnis 2001).

    The rate of primary charge separation in PSI is
assumed to be

$$v_{bf15} = k_{15}[P_{700e}] \frac{[A_0]}{[A_{0T}]} \tag{31}$$

where $[A_0]/[A_{0T}]$ is the proportion of open primary accep-
tors of PSI, k_{15} is the rate constant for PSI primary charge
separation, which was calculated based on a half-time
($t_{1/2}$) of 30 ps (Chitnis 2001).

16 Electron transport from A_0^- to ferredoxin

$$2A_0^- + Fd \leftrightarrow Fd^{2-} + A_0$$
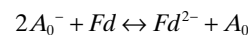
The half-time ($t_{1/2}$) for electron transfer from A_0 to ferre-
doxin was assumed to be 200 ns and this is incorporated
into k_{16} below (Chitnis 2001). The rate equation for this
reaction is

$$v_{bf16} = k_{16}[A_0^-] \frac{[Fd]}{[Fd_T]} \tag{32}$$

where $[Fd_T]$ is the total concentration of ferredoxin
($[Fd_T] = [Fd] + [Fd_r]$) where $[Fd]$ and $[Fd_r]$ are the con-
centrations of oxidized and reduced ferredoxin,
respectively.

17 The formation of NADPH
The detailed kinetics of the electron transfer process
between Fd_r and $NADP^+$ are not known. Fd has been
suggested to form a rigid complex with ferredoxin-NADP
reductase (FNR) (Laisk *et al.* 1992; Laisk 1993; Lelong
et al. 1994). Since electron transfer reactions are usually
very fast in this complex, as a simplification, in *e*-
photosynthesis, it is assumed that availability of $NADP^+$
is the limiting step for generation of NADPH. A simple
one-substrate one-product Michaelis–Menten rate equa-
tion is therefore used to describe this reaction, as in Frid-
lyand *et al.* (1999):

$$v_{bfn2} = \frac{V_{2M}\left(\frac{[Fd_r]}{[Fd_T]}[NADP^+] - \frac{[Fd]}{[Fd_T]}\frac{[NADPH]}{K_2}\right)}{K_{mNADP}\left(1 + \frac{[NADP^+]}{K_{mNADP}} + \frac{[NADPH]}{K_{mNADPH}}\right)} \tag{33a}$$

where v_{bfn2} is the rate of this reaction, K_{mNADP} and
K_{mNADPH} are the Michaelis–Menten constants for *NADP*

and *NADPH*, respectively, V_{2M} is the maximum rate of
the forward reaction, K_2 is the equilibrium constant for
this reaction, which is determined by the difference in
redox potential between Fd/Fd_r (about –0.420 V) and
NADP/NADPH (about –0.340 V) at pH 8 (Keirns &
Wang 1972; Knaff 1996). Following Fridlyand *et al.* (1999),
the maximum rate of electron transfer from Fd_r to *NADP*
is 1600 e^- s^{-1}, which corresponds to a maximum rate of
NADPH generation of 27.8 mmol L^{-1} s^{-1} based on the
assumed ferredoxin concentration and standard dimen-
sions of leaf and chloroplasts used in the model.

18 Cyclic electron transfer
In *e*-photosynthesis, we assume that the cyclic electron
transfer is continuously engaged (Joliot & Joliot 2002).
Though there are various proposed mechanisms of cyclic
electron transfer (Bendall & Manasse 1995; Shikanai
2007). Here we assume the simplest and widely accepted
model that the electron transfer to the plastoquinone
bound to the Q_n site is rate dependent on the redox state
of the ferredoxin and concentration of plastoquinone
bound to the Q_n site $[PQ_n]$:

$$v_{cet} = V_{cetm}[PQ_n][Fd_r]/[Fd_T] \tag{33b}$$

where V_{cetm} is the maximal rate of cyclic electron transfer.
By setting V_{cetm} to zero, the model will simulate a photo-
synthetic apparatus with no cyclic electron transfer.

Rate equations associated with regulatory mechanisms

Reactions associated with NPQ

The mechanism of NPQ proposed by Crofts & Yerkes (1994)
is incorporated into the model (See the section, *Model struc-
ture and assumptions used in the model*). In summary, this
assumes that decrease in lumenal pH increases the protona-
tion of a putative ligand (q_{H+}) causing a conformational
change in the quenching site in turn increasing the rate con-
stant for of heat dissipation (k_d). The pK_a value of the puta-
tive ligand is assumed to be 4.5 (Gilmore 1997). A differential
equation describing the rate of change in k_d (Laisk *et al.* 1997)
is used:

$$\frac{dk_d}{dt} = k_r(q_{H+} \cdot k_{dm} - k_d) \tag{34}$$

where:

$$q_{H+} = \frac{[H_{fl}]}{[H_{fl}] + K_E} \tag{35}$$

$$K_E = 10^{-pK} \tag{36}$$

where $[H_{fl}]$ is the proton concentration in lumen, k_{dm} is the
maximum rate constant for heat dissipation and k_r describes
the rate of relaxation of the rate constant of heat dissipation.

Activation of Rubisco by Rubisco activase

The order of substrate binding is critical for normal functioning of Rubisco. Rubisco is carbamylated by forming a complex with CO_2 and Mg^{2+}. Carbamylated Rubisco can bind RuBP and in turn CO_2 or O_2 leading to carboxylation or oxygenation (Fig. 1b). If, however, Rubisco binds RuBP before binding CO_2 and Mg^{2+} (uncarbamylated), is assumed to be inactive. Rubisco activase increases the rate constant for the release of RuBP minimizing this inactivation (Portis 1995, Portis, 2003). These processes were explicitly incorporated into e-photosynthesis. The detailed equations describing the reactions involved in Rubisco activation and deactivation (Fig. 1b) are given in Supporting Information Appendix S3 section 1.1. The key assumptions are described here. Following Mott & Woodrow (2000), the rate constant for activating Rubisco (k_{ra}) is

$$k_{ra} = \frac{[\text{activase}]}{13014} \qquad (37)$$

where [activase] represents the concentrations of Rubisco activase for which 13014 s mg [activase] m^{-2} is an empirically derived constant (Mott & Woodrow 2000).

The activity of Rubisco activase is assumed to be regulated by the ratio of stromal ADP to ATP concentrations, following Zhang & Portis (1999).

The rate of RuBP dissociation from Rubisco (v_{ra1}) is calculated as

$$v_{ra1} = k_{ra}[ER] \cdot \max\{(1-[ADP]/(3[ATP])), 0\} \qquad (38)$$

where $[ER]$ is the concentration of RuBP bound to Rubisco.

The rate of formation of $[ER]$ (v_{ran1}) is assumed to follow mass action:

$$v_{ran1} = k_{n1}[E][RuBP] \qquad (39)$$

where k_{n1} is based on the reported time needed for Rubisco inactivation (Ernstsen, Woodrow & Mott 1999).

In the model, $[E]$, $[EC]$ and $[ECM]$ remain in equilibrium (Fig 1b) using the equilibrium constants of Mate *et al.* (1996). The rate of formation of ECMR, that is, carbamylated Rubisco with bound RuBP and Mg^{2+}, is calculated as

$$v_{ra7} = k_{ra7}[ECM][RuBP] \qquad (40)$$

There are no measurements for this rate constant but since it is assumed not to be rate limiting, k_{ra7} was set to 10 times the catalytic number for carboxylation by active sites of Rubisco, giving 25 s^{-1}.

The rate of RuBP dissociation from ECMR has been found to be very slow compared to the rate of catalytic conversion of ECMR to PGA (Portis 1995), this observation was approximated in the model by assuming a dissociation constant (k_{ran7}) of 0.5 s^{-1}:

$$v_{ran7} = k_{ran7}[ECMR] \qquad (41)$$

The xanthophyll cycle

The xanthophyll cycle, which involves interconversion among zeaxanthin (Zx), antheroxanthin (Ax) and violaxanthin (Vx), is critical for photoprotection of the photosynthetic apparatus by the thermal dissipation of absorbed energy. It is assumed that the interconversions among Vx, Ax and Zx follow first-order kinetics (Eqns 42–45). The initial concentrations of Vx, Ax and Zx as well as the rate constants for conversions of Vx to Ax and of Ax to Zx were from experimentally determined values (Frommolt, Goss & Wilhelm 2001; Table 2.4 in Supporting Information Appendix S2). The influence of changes in lumenal pH on the rate constants of conversion from Vx to Ax, and from Ax to Zx was described by assuming the rate constants of Vx to Ax, and from Ax to Zx are at their maximum when lumenal pH is lower than 5.2 (Frommolt *et al.* 2001) and that these two rate constants decrease linearly when lumenal pH is higher than 5.2 reaching zero at pH $\geq$ 6.5 (Supporting Information Appendix S3; section 1.1). X_{state}, defined as $[Zx]/([Ax]+[Vx]+[Zx])$, was used to predict the maximum rate constant of heat dissipation (d_m). The maximal rate 'constant' for heat dissipation (k_{dm}) is inversely related to X_{state} (Eqns 34–36, 48). The sum of $[Ax]$, $[Vx]$ and $[Zx]$ is assumed constant throughout. Although referred to as a rate constant (k_d), this apparent rate constant will vary. Here we assume this variation may be described via dynamics of zeaxanthin concentration and luminal pH. Demmig-Adams & Adams (1996) quantified the impacts of xanthophyll cycle components on heat dissipation rate constant. As an approximation, this model assumes a minimum k_{dm} at $X_{state} \leq 0.3$, defined by k_{d0}. At $X_{state} > 0.3$, k_{dm} is increased as a function of X_{state}, divided by 0.3 so that k_{dm} will never be less than k_{dm0} and will be increased by about 3.3 times when X_{state} becomes 1 (Eqn 48). Change in the k_r is similarly calculated (Eqn 49). These values of k_r and k_{dm} are then substituted into Eqn 34 to simulate the dual effects of X_{state} and pH on k_d.

$$v_{av} = [Ax]k_{av} \qquad (42)$$

$$v_{va} = [Vx]k_{va}pHReg \qquad (43)$$

$$v_{az} = [Ax]k_{az}pHReg \qquad (44)$$

$$v_{za} = [Zx]k_{za} \qquad (45)$$

$$\begin{aligned} pHReg &= 1 \quad (pH_l <= 5.8) \\ pHReg &= \frac{6.5 - pH_l}{0.7} \quad (6.5 > pH_l >= 5.8) \\ pHReg &= 0 \quad (pH_l > 6.5) \end{aligned} \qquad (46)$$

$$X_{state} = \frac{[Zx]}{[Ax]+[Vx]+[Zx]} \qquad (47)$$

$$k_{dm} = k_{dm0} \max\{X_{state}/0.3, 1\} \qquad (48)$$

$$k_{r} = k_{r0} \max\{X_{state}/0.3, 1\} \qquad (49)$$

Regulation of enzyme activity via thioredoxin

e-Photosynthesis incorporates thioredoxin regulation of sedoheptulose-1:7-bisphosphatase (SBPase), fructose-1:6-bisphosphatase (FBPase), phosphoribulose kinase (PRK), glyceraldehyde-3-phosphate dehydrogenase (GAPDH), ADP-glucose pyrophosphorylase (ADPGPP), rubisco activase (activase) and ATP synthase (ATPase). Thioredoxin regulates the activities of these enzymes by thiol/disulfide exchange, reducing disulfide (-s-s-) on the inactive form of an enzyme to sulfhydryl (–SH) groups yielding the active enzyme and vice-versa (Schurmann & Buchanan 2001). A standard rate equation describing electron transfer reactions between two redox components was used to describe the electron transfer between enzymes and thioredoxin (Laisk & Walker 1989; Chang 2000). For example, the electron transfer rate from thioredoxin to phosphoribulose kinase (PRK) (v_{e2PRK}) is calculated as:

$$v_{e2PRK} = k_{e2PRK}\left([Thio_{r}][PRK_{o}] - \frac{[Thio_{o}][PRK_{r}]}{KE_{2PRK}}\right) \qquad (50)$$

where k_{e2PRK} is the rate constant of electron transfer from reduced thioredoxin ($Thio_{r}$) to oxidized *PRK* (PRK_{o}). [PRK_{r}] and [$Thio_{o}$] represent the concentrations of reduced PRK and oxidized thioredoxin, respectively. KE_{2PRK} represents the equilibrium constant of the electron transfer between thioredoxin and *PRK*, which was estimated based on the difference between midpoint potentials of thioredoxin and *PRK* (Eqn 6). The redox potentials and concentrations of these different enzymes, rate constants of electron transfer from thioredoxin to these different enzymes were obtained from literature (Supporting Information Appendix S2, Table 2.2) Thioredoxin was reduced subsequently by ferredoxin via ferredoxin-thioredoxin reductase (Supporting Information Appendix S3, section 1.1).

MODEL REPRESENTATION AND ALGORITHMS

e-Photosynthesis, combines all reactions in the model of carbon metabolism (Zhu *et al*. 2007), the model of fluorescence induction (Zhu *et al*. 2005), as well as the electron transfer reactions around cyt b₆f and PSI, ATP and NADPH generation, as well as the regulatory mechanisms described above. The procedure used in building the model of carbon metabolism and fluorescence induction (Zhu *et al*. 2005, 2007; Zhu 2010) was used here to achieve *e*-photosynthesis. The system of ordinary differential equations representing the structure of *e*-photosynthesis was solved numerically using *ode15s* of MATLAB (v6, the Mathworks, Inc, Natick, MA, USA). The structural and kinetic properties of enzymes/components used in *e*-photosynthesis were collected from the peer reviewed literature (Supporting Information Appendix S2, Tables 2.1 to 2.3).

NUMERICAL EXPERIMENTS

The initial concentrations of components in photosynthesis were based on those in a representative sunlit leaf of an herbaceous C3 dicot (see Zhu *et al*. 2005; Zhu *et al*. 2007; Supporting Information Appendix S2, Tables 2.4 and 2.5).

Experiment 1

An *in silico* perturbation experiment was conducted to investigate the ability of *e*-photosynthesis to attain a steady state and reliably regain that steady state after a simulated environmental perturbation. Specifically, in the model, steady state was attained at a photosynthetically active photon flux density (PFD) of 1000 μmol m^{-2} s^{-1}. Then after 200 s, PFD was decreased to 100 μmol m^{-2} s^{-1} for 200 s, and then returned to 1000 μmol m^{-2} s^{-1}.

Experiment 2

To assess the criticality of specific model parameters, a sensitivity analysis was conducted. Parameters were individually decreased by 20% and 80%, under low and high light, and under current and elevated atmospheric [CO_2].

Experiment 3

e-Photosynthesis was tested for its ability to reproduce typical responses of leaf CO_2 uptake to intercellular CO_2 concentration (A/c_i curve) and to PFD (A/PFD curve). These were obtained by working stepwise through a range of c_i and of PFD, allowing a steady-state *A* to be achieved at each step.

Experiment 4

e-Photosynthesis was examined for its ability to mimic modulated chlorophyll fluorescence quenching. A typical *in vivo* quenching analysis protocol was used as described in the legend of Fig. 6.

RESULTS

Experiment 1

Despite rate constants in the system of differential equations spanning 11 orders of magnitude, the system successfully attained a steady state, regained a new steady state following a 10-fold decrease in PFD, and then successfully returned to the original steady state when returned to the original PFD (Fig. 2). Further, *e*-photosynthesis gave quantitatively and temporally realistic predictions of the dynamics of CO_2 uptake (*A*), O_2 evolution, heat dissipation and the quantum yield of PSII (Φ_{PSII}), chlorophyll fluorescence, membrane potential, lumenal and stromal pH (Fig. 2). For example, the predicted *A* of 15 and 5 μmol m^{-2} s^{-1} at 1000 and 100 μmol m^{-2} s^{-1} under current CO_2 and O_2 levels are within the range of commonly measured *A* for a healthy C3 leaf (Wullschleger 1993). Furthermore, the increase in the
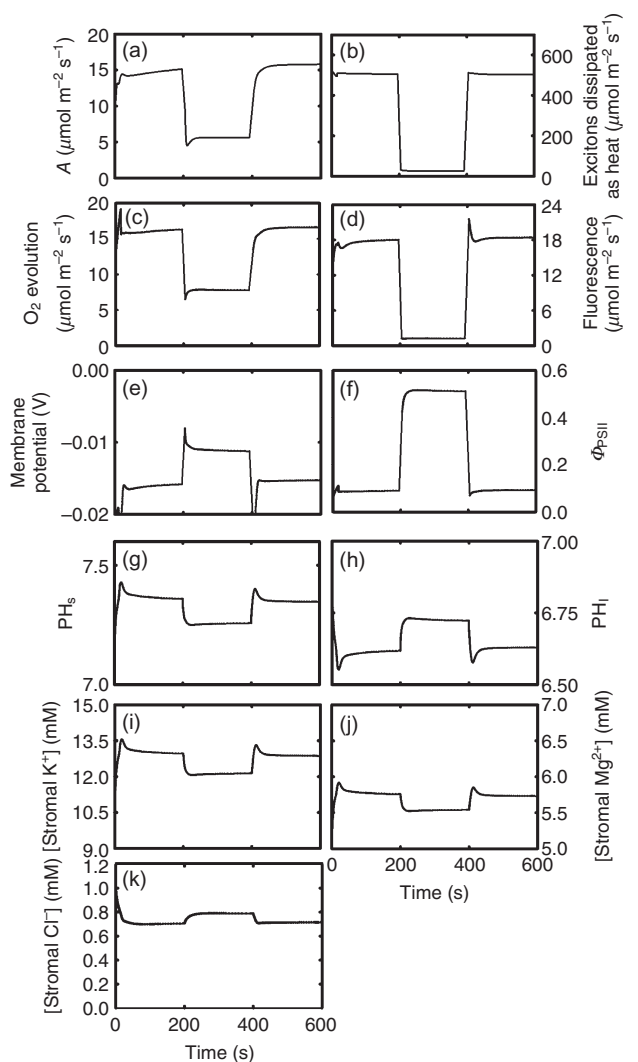
Figure 2. Predicted responses of photosynthesis and chloroplast properties in response to a 10-fold reduction in photon flux density (PFD) and return to the original PFD. The structural and kinetic properties of enzymes or components used in *e*-photosynthesis (Tables 2.2 and 2.3 in Supporting Information Appendix S2) are based on literature for a 'typical' terrestrial C3 leaf, as described previously Zhu *et al.* (2005, 2007). The initial concentrations of different intermediates and parameters are given in Tables 2.4 and 2.5 of Supporting Information Appendix S2. Intercellular CO_2 and O_2 concentrations were set to be 280 μmol mol^{-1} and 210 mmol mol^{-1}, respectively. Temperature was 25 °C and PFD 1000 μmol m^{-2} s^{-1} for 0–200 s, 100 mol m^{-2} s^{-1} for 200–400 s, returning to 1000 μmol m^{-2} s^{-1}. (a) Net leaf photosynthetic CO_2 uptake rate (*A*); (b) 'excitons' dissipated as heat, (c) the rate of O_2 evolution by photosystem II (PSII); (d) chlorophyll fluorescence; (e) membrane potential; (f) quantum yield of PSII; (g) stromal pH; (h) lumenal pH; (i) stromal [K$^+$]; (j) stromal [Mg^{2+}]; and (k) stromal [Cl$^-$].

proportion of excitation energy dissipated as heat (Fig. 2b) and a decrease in quantum yield of PSII under high light (Fig. 2f) are consistent with vast amount of experimental observations as well; see reviews in (Long, Humphries & Falkowski 1994; Horton *et al.* 1996; Ort 2001).

Experiment 2

Sensitivity analysis: unsurprisingly, the predicted steady state rate of net CO_2 uptake (*A*) was very sensitive to the assumed number of protons required to produce one ATP (Table 1). At high [CO_2] and PFD, assuming 4 in place of 4.67 increased *A* by 22%. At low light, decreasing other parameters by 20% had little effect on the predicted *A*; however, decreasing ATP/H$^+$ had a very significant effect (Table 1). This is consistent with expectation since under light-limiting conditions, the efficiency of energy transduction into NADPH and ATP will be critical to the overall rate of photosynthesis. Of the 11 further parameters tested, only a 20% decrease in the concentrations of FBPase, SBPase, Cyt b$_6$f and Rubisco caused a decrease in *A* in high light (Table 1). At elevated [CO_2] similar decreases were observed excepting that *A* became insensitive to a 20% decrease in Rubisco, which is consistent with the fact that this enzyme is more efficient as [CO_2] is increased (e.g. Long *et al.*, 2004). When decreased by 80%, FBPase, SBPase, Rubisco, Cyt b$_6$f and ATP synthase caused c. 40–75% reductions in *A*, in high light and at both levels of [CO_2]. The rate of formation of carbamylated Rubisco (ECM) with RubP is determined by the rate constant k_{ra7}. No clear value of this critical rate constant was available. This analysis showed that k_{ra7} inserts little control over photosynthetic CO_2 uptake under both current and future elevated [CO_2] (Table 1).

Experiment 3 and 4

In a simulated experiment, leaf photosynthesis was allowed to achieve steady state at a PFD of 1000 μmol m^{-2} s^{-1}, and then PFD was decreased by a step of 100 μmol m^{-2} s^{-1} every 200 s, achieving a new steady-state, before each decrease. Changes in all parameters and quantitative values, for example, the CO_2 uptake rate and oxygen evolution rate, generally reflect those typically seen in conducting such experiments in healthy C3 leaves (Fig. 3; von Caemmerer 2000). When the data are used to reconstruct the response of *A* to PFD, a typical response curve may be seen with an initial linear response to PFD in low light and saturation at about 500 μmol m^{-2} s^{-1} (Fig. 3j). Similarly, an experiment in which the response of *A* in saturating light to intercellular [CO_2] was simulated by running photosynthesis to steady state at a c_i of 1000 μmol mol^{-1} and then decreasing c_i in steps of 100 μmol mol^{-1} at 200 s intervals, allowing steady state to be achieved in each step (Fig. 4). Again, the response pattern and quantitative value of key measures are consistent with those observed *in vivo*. When the data are used to reconstruct the response of *A* to c_i, a typical response curve of a light-adapted C3 leaf may be seen with a high dA/dc_i at low c_i where photosynthesis is RuBP saturated and declining to near saturation at a c_i above c. 300 μmol mol^{-1} (Fig. 4j).

Experiment 5

Leaf photosynthesis was allowed to reach steady state at a PFD of 2000 μmol m^{-2} s^{-1} and c_i of 280 μmol mol^{-1}, and

Table 1. Sensitivity analysis of chosen parameters in *e*-photosynthesis on photosynthetic CO_2 uptake rate ($\mu mol\ m^{-2}\ s^{-1}$)

	[CO$_2$] (μmol mol^{-1})	280		560	
Scaling coefficient 1	PFD (μmol m^{-2} s^{-1})	200	2000	200	2000
	Control	8.34	15.9	10.6	20.82
HPR = 4	HPR	8.91	17.3	11.31	25
Decrease by 20%	[FBPase]	8.32	15.5	10.6	20.26
	[SBPase]	8.3	15.8	10.6	20.67
	[Cyt b$_6$f]	8.34	15.2	10.6	19.88
	[Fd$_T$]	8.34	15.9	10.6	20.8
	[P$_{700T}$]	8.34	15.9	10.6	20.8
	[ATP synthase]	8.3	15.9	10.6	20.8
	[PSII centre]	8.34	15.9	10.6	20.8
	[activase]	8.34	15.9	10.6	20.8
	[OEC]	8.34	15.9	10.6	20.8
	kra7	8.34	15.9	10.6	20.8
	[Rubisco]	8.4	14.46	10.68	20.8
Decrease by 80%	[FBPase]	4.16	4.46	5.25	5.34
	[SBPase]	7.33	9.72	9.36	12.47
	[Cyt b$_6$f]	7.05	6.99	8.96	9.17
	[Fd$_T$]	8.34	15.9	10.61	20.82
	[P$_{700T}$]	8.34	15.9	10.61	20.82
	[ATP synthase]	6.74	6.89	8.55	8.6
	[PSII centre]	8.34	15.9	10.61	20.82
	[activase]	8.34	15.9	10.61	20.82
	[OEC]	8.34	15.9	10.61	20.82
	kra7	8.34	15.9	10.7	20.8
	[Rubisco]	3.7	3.79	6.52	6.61

The photosynthetic CO_2 uptake rate is calculated as the rate of RuBP carboxylation minus the rate of CO_2 release by glycine decarboxylase. The sensitivity analysis was conducted by decreasing the default parameter values by either 20% or by 80%. The sensitivity analysis was conducted for intercellular CO_2 concentrations corresponding to current (280 μmol mol^{-1}) and elevated CO_2 concentrations (560 μmol mol^{-1}) under low (200 μmol m^{-2} s^{-1}) and high (2000 μmol m^{-2} s^{-1}) PFDs.

returned to darkness. After a brief period, the leaf was returned to a PFD of 2000 μmol m^{-2} s^{-1} and induction and quenching of chlorophyll fluorescence was tracked and analysed with simulated saturating light flashes. Figure 5 shows the initial fluorescence transient and Fig. 6 analyses this further with a series of saturating flashes. Fluorescence transients show the typical OPMST series of transients in emission (Fig. 5). On dark-light transition, a burst of O_2 release is indicated and a prompt rise in fluorescence followed by quenching, coupled with a rise in NPQ (Fig. 6) mimicking typically observed changes in leaf chlorophyll fluorescence *in vivo*.

DISCUSSION

The induction of photosynthesis following a dark to light transition was realistically simulated showing a gradual increase in *A* upon illumination (Fig. 2a), which was the result of gradual activation of different enzymes involved in the C3 cycle, that is, SBPase, PRK, GAPDH, ADPGPP and Rubisco activase by the ferredoxin-thioredoxin system (Schurmann & Jacquot 2000). One caveat is that induction of *A* was complete within about 200 s. In an intact leaf, complete induction typically requires more time; however, this is likely due to the slower opening of the stomata. The current version of *e*-photosynthesis does not include stomatal dynamics or

any diffusive limitation to CO_2 access to the stroma. However, this length of induction is consistent with rates observed in isolated protoplasts of wheat mesophyll cells, which would not be affected by stomatal and other diffusive limitations. Here, steady state was achieved within 240 s of a dark-light transition (Leegood & Walker 1981).

Oscillations in CO_2 uptake and O_2 evolution, which have often been observed in leaves following rapid changes in light and CO_2 levels (Walker 1992), were predicted by *e*-photosynthesis when PFD was abruptly changed (Fig. 2a,c). At a low light level (100 μmol m^{-2} s^{-1}), the resting membrane potential is about −11 mV; decreasing to about −15 mV under high light level (1000 μmol m^{-2} s^{-1}) after 200 s (Figs 2e & 3e). This change in the trans-membrane electrical potential was caused by changes in the concentration of charged ions ($Mg^{2+}, K^+, Cl^-, H^+, OH^-$) between the lumen and stroma. More specifically, the change in trans-membrane potential under high light is caused by an increase in lumenal [H^+] counteracted by decreases in concentrations of lumenal Mg^{2+}, K^+ and increase in concentration of lumenal Cl^- (Fig. 2i,j,k). These changes are consistent with observed ion fluxes across the thylakoid membranes of intact leaves (Vredenberg & Bulychev 1976) and in isolated chloroplast (Cruz *et al*. 2001) in dark to light transitions (c.f. Flores *et al*. 1983; Kramer, Dimarco & Loreto 1995; Kramer *et al*. 1999; Cruz *et al*. 2001; Kramer, Cruz & Kanazawa 2003).
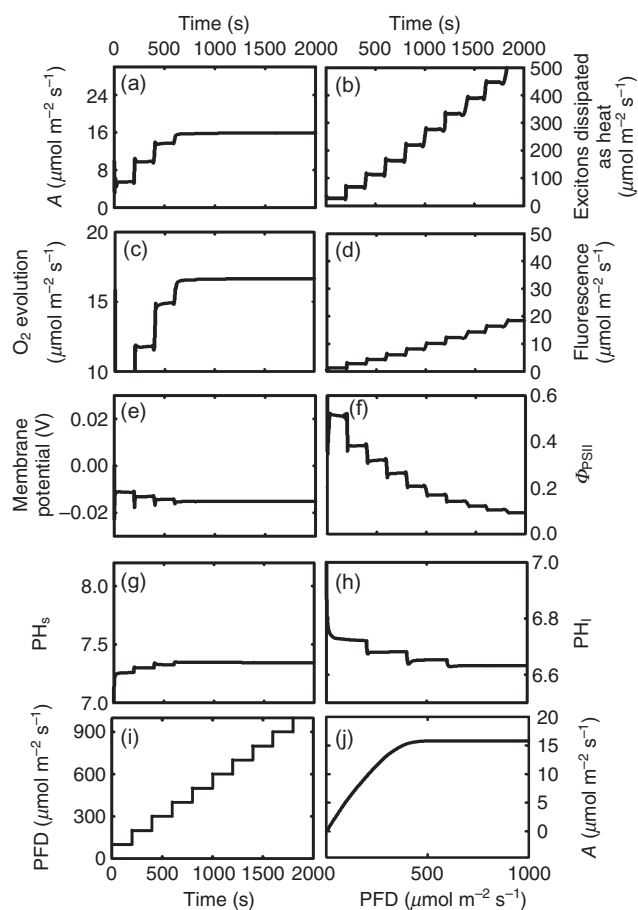
Figure 3. The predicted response of photosynthesis to photon flux density (PFD) in terms of (a) net leaf photosynthetic CO_2 uptake rate (A); (b) 'excitons' dissipated as heat; (c) the rate of O_2 evolution by photosystem II (PSII); (d) chlorophyll fluorescence; (e) membrane potential; (f) quantum yield of PSII; (g) stromal pH; and (h) lumenal pH. Here, the leaf was transferred from darkness to a PFD of 100 μmol m^{-2} s^{-1}, which was maintained for 200 s, and then increased by a further 100 μmol m^{-2} s^{-1}, with steady state being achieved before the end of 200 s at each step. These step increases were continued at 200 s intervals until 1000 μmol m^{-2} s^{-1} was attained (panel i). A response curve of A to PFD is reconstructed from the data of panel A (panel j). The x-axis of all panels is time (s), except panel j, where the x-axis is PFD. Apart from variation in PFD, all other conditions for simulations were as in Fig. 2.

e-Photosynthesis provided realistic predictions of the responses of steady-state A to PFD (A-PFD response, Fig. 3) and to c_i (A-c_i response, Fig. 4). The A-c_i and A-PFD curves have been used extensively to probe the limitation of photosynthesis, either by RuBP carboxylation or RuBP regeneration (Farquhar *et al*. 1980). To construct the A-PFD curve (Fig. 3a), each PFD was maintained for 200 s with increments of 100 μmol m^{-2} s^{-1} from 100 to 1000 μmol m^{-2} s^{-1} (Fig. 3i). At PFD below 500 μmol m^{-2} s^{-1}, steady-state A increased almost linearly with increasing PFD, consistent with a dominating RuBP regeneration limitation, in line with the widely validated steady-state biochemical model of photosynthesis of Farquhar *et al*. (1980). Beyond 500 μmol m^{-2} s^{-1}, increases in

PFD resulted in only slight increases in A consistent with RuBP carboxylation rate as the major limitation to A in high light (Fig. 3a), again in line with Farquhar *et al*. (1980). With increases in PFD, the amount of energy dissipated by heat gradually increased (Fig. 3b). The predicted increased heat dissipation through NPQ is expected in order to protect PSII from damage by excessive excitation (Fig. 3b) (Long *et al*. 1994; Horton *et al*. 1996; Ort 2001).

The response of A to c_i was simulated by attaining steady-state photosynthesis at a c_i of 1000 μmol mol^{-1} and then decreasing c_i in 100 μmol mol^{-1} increments each maintained for 200 s, until c_i reached 100 μmol mol^{-1} (Fig. 4i). Consistent with the steady-state model of Farquhar *et al*. (1980), for a light-adapted leaf A declined slowly with decrease in c_i until
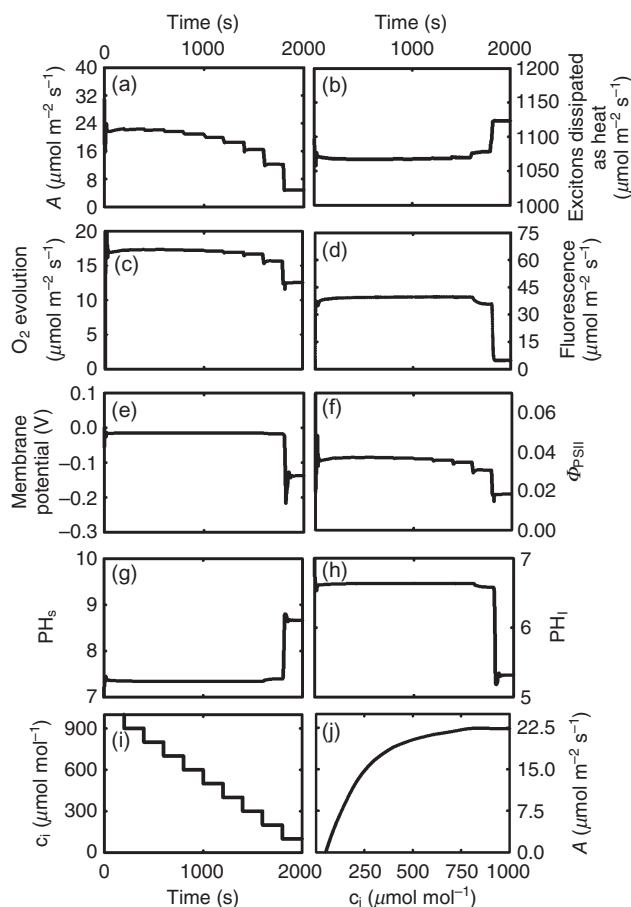

Figure 4. The predicted response of photosynthesis to intercellular CO_2 concentration (c_i) in terms of (a) net leaf photosynthetic CO_2 uptake rate (A); (b) 'excitons' dissipated as heat; (c) the rate of O_2 evolution by photosystem II (PSII); (d) chlorophyll fluorescence; (e) membrane potential; (f) photosystem II (PSII) electron transfer rate; (g) stromal pH; and (h) lumenal pH. Here, the initial leaf c_i was set at 1000 μmol mol^{-1} for 200 s, and then decreased in steps of 100 μmol mol^{-1} every 200 s until 100 μmol mol^{-1} was attained (panel i). A response curve of A to c_i is reconstructed from the data of panel A (panel j). The x-axis of all panels is time (s), except panel j, where the x-axis is c_i. Apart from variation in c_i and use of a photon flux density (PFD) of 1000 μmol m^{-2} s^{-1}, throughout, all other conditions for simulations were as in Fig. 2.
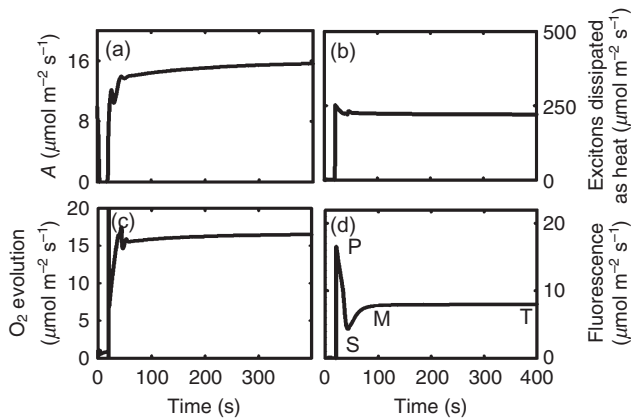
Figure 5. Simulated chlorophyll fluorescence induction and quenching, showing PMST kinetics with P representing the intial peak of fluorescence after initial illumination, S representing a semi-steady state, M representing a possible maximum fluorescence after S and T representing a terminal steady state (Papageorgiou, 1975) (panel d), and parallel changes in (a) net leaf photosynthetic CO_2 uptake rate (A); (b) heat dissipation and (c) the rate of O_2 evolution by photosystem II (PSII). The photon flux density (PFD) of the actinic light was 500 μmol m^{-2} s^{-1}. Intercellular [CO_2] is 280 μmol mol^{-1} and [O_2] is 210 mmol mol^{-1}. The measurement light PFD was 7 μmol m^{-2} s^{-1}. The actinic light of 500 μmol m^{-2} s^{-1} was added at the 20th second.

Chlorophyll fluorescence decay curve

Fluorescence induction (FI) includes both rise and decay components each of which are composed of characteristic phases (e.g. Govindjee 1995). Compared to the number of studies regarding the mechanisms of the OJIP phases of the FI rise (Stirbet *et al*. 1998; Lazar 2003; Zhu *et al*. 2005; Lazar & Schansker 2009), relatively less theoretical effort has been made to explore the mechanisms of PSMT decay phases. This is no doubt because PSMT results from a more diverse set of processes compared to the initial OJIP, and critically depends on the whole electron transfer processes and the dynamics of carbon metabolism. Since *e*-photosynthesis incorporates these processes, a critical test of the model is its ability to simulate the well established PSMT decay phase, and

simulated measurement of J_{PSII} during this phase with saturating light flashes. Previously, we have shown that the OJIP induction can be realistically simulated (Zhu *et al*. 2005), here we show a temporally realistic simulation by *e*-photosynthesis of the PSMT phase as a result of connecting PSII processes with downstream electron transport, thylakoid membrane chemical concentration and electrical potential gradients, and carbon metabolism. Transition from M to T was consistent with attainment of steady-state A, O_2 evolution associated with whole-chain electron transport and heat dissipation (Fig. 5). Fluorescence induction phases OJIPSMT can be easily and rapidly measured in intact leaves. They provide a potential means for high-throughput screening, for example, of the progeny of crosses. However, a barrier to their application has been an understanding of the relationship of these transients to factors, which actually affect productivity and environmental tolerance. *e*-Photosynthesis therefore provides a theoretical framework for determining and testing hypotheses about the underlying processes causing variation in these easily measured transients in the fluorescence induction curve.

Use of saturating pulses of light coupled with measurement of modulated chlorophyll fluorescence has emerged as the major method for determining J_{PSII} and NPQ during induction and during steady-state photosynthesis in intact
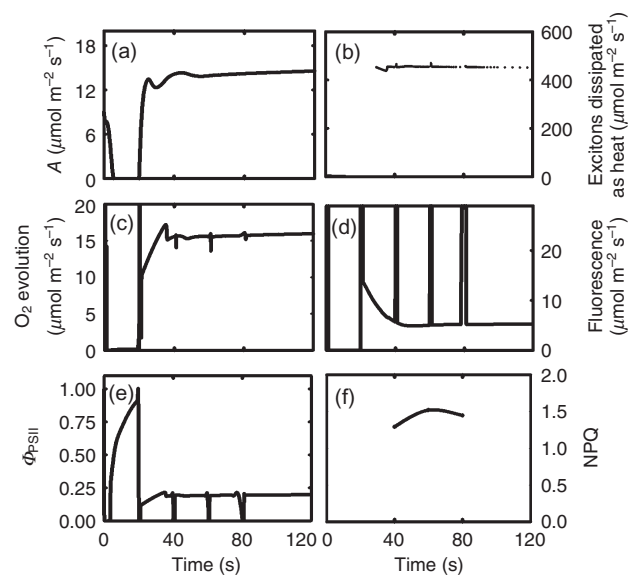
about 300 μmol mol^{-1}, after which A declines rapidly, reflecting the transition from RuBP-limited to RuBP-saturated photosynthesis (Fig. 4a). When photosynthesis is RuBP-limited, decrease in A with decrease in c_i results simply from increased partitioning of RuBP and electrons to C2 metabolism, which is consistent with the small change in both J_{PSII} (Fig. 4f) and O_2 evolution associated with whole-chain electron transport (Fig. 4c), followed by much larger declines at $c_i < 400$ μmol mol^{-1}, as CO_2 supply limitation slows the utilization of the products of whole-chain electron transport. In Fig 4a, leaf CO_2 uptake decreases more with decreases in c_i than does O_2 evolution. This is because O_2 evolution here and in other figures is simply attributed to whole-chain electron transport and is not corrected for photorespiratory and dark respiratory fluxes.

Figure 6. A simulated analysis of chlorophyll fluorescence quenching using a series of saturating flashes. A photon flux density (PFD) of 1 μmol m^{-2} s^{-1} was 'applied' between 0 and 20th second, then, a saturating pulse with PFD of 8000 μmol m^{-2} s^{-1} was 'applied' between 20 and 21st second. An actinic light with PFD of 500 μmol m^{-2} s^{-1} was 'applied' 200 s later, and saturating flashes of 8000 μmol m^{-2} s^{-1} and 1 s duration 'applied' at 5 s intervals. Intercellular [CO_2] was 280 μmol mol^{-1} and [O_2] is 210 mmol mol^{-1}. Panels show the responses of (a) photosynthetic CO_2 uptake rate (A); (b) 'excitons' released as heat; (c) the rate of O_2 evolution by photosystem II (PSII); (d) chlorophyll fluorescence; (e) the quantum efficiency of electron transport through PSII (Φ_{PSII}); and (f) non-photochemical quenching (NPQ).

leaves. As a further test of *e*-photosynthesis, such measurements were simulated starting with application of a saturating flash to a dark-adapted leaf, and then followed by a sequence of flashes through induction of photosynthesis. This yielded temporally and quantitatively realistic patterns of the emergence of chlorophyll fluorescence quenching, NPQ, heat dissipation and Φ_{PSII} during induction of *A* following a dark-light transition (Fig. 6).

CONCLUSIONS

Photosynthesis is almost unique among biological processes in the rich array of external signals that may be measured, thereby allowing screening or imaging of large numbers of plants. Lacking, however, has been a comprehensive theoretical framework for assessing and interpreting these signals used in combination. *e*-Photosynthesis now provides a workable platform. Although this model is perhaps the most comprehensive to date, it is far from complete. Many further feedback and feedforward controls surely exist. However, the outcomes of the simulations show that the existing knowledge incorporated into this mechanistic model is sufficient to reproduce widely observed *in vivo* responses of photosynthesis to environmental perturbations. The model now provides a framework for informed engineering of improved photosynthetic efficiency. It also provides a means to interpret gas exchange, fluorescence and absorption spectroscopy more fully and from a mechanistic basis. This in turn could improve the value of these measures in the development of high-throughput screening for the emerging phenomics field. The *e*-photosynthesis model provides a critical module for a dynamic systems model of canopy photosynthesis as well (Zhu, Song & Ort 2012). Finally, as demonstrated in the sensitivity analysis, the model provides a quantitative assessment of strengths and weaknesses of current understanding of the photosynthetic system as a whole.

Inevitably improved parameters and equations representing the >100 steps of this model will be developed and complete parameter sets will become available for individual plants. To this extent, *e*-photosynthesis is intended as a 'living' model available to be improved by the community.

Availability

This model is available for research and teaching upon request from authors. The model can be freely used for academic purposes. For commercial purposes, special commercial license is required.

ACKNOWLEDGMENT

REFERENCES

Barber J. (1976) Ionic regulation in intact chloroplasts and its effect on primary photosynthetic processes. In *The Intact Chloroplast* (ed. J. Barber), pp. 89–134. Elsevier/North-Holland Biomedical Press, Amsterdam.

Beadle C.L. & Long S.P. (1985) Photosynthesis – is it limiting to biomass production. *Biomass* **8,** 119–168.

Bendall D.S. & Manasse R.S. (1995) Cyclic photophosphorylation and electron transport. *Biochimica et Biophysica Acta-Bioenergetics* **1229,** 23–38.

Berry E.A., Guergova-Kuras M., Huang L.S. & Crofts A.R. (2000) Structure and function of cytochrome bc complexes. *Annual Review of Biochemistry* **69,** 1005–1075.

Bockris J.O.M. & Reddy A.K.N. (1970) *Modern Electrochemistry*, Vol. **1.** Plenum Press Corp, New York.

Bowyer J.R., Tierney G.V. & Crofts A.R. (1979a) Cytochrome c_2-reaction center coupling in chromotophores of *Rhodopseudomonas sphaeroides* and *Rhodopseudomonas capsulata*. *FEBS Letter* **101,** 207–212.

Bowyer J.R., Tierney G.V. & Crofts A.R. (1979b) Secondary electron transfer in chromotophores of *Rhodopseudomonas capsulata* Ala pho⁺. Binary out-of-phase oscillations in ubisemiquinone formation and cytochromic b_{50} reduction with consecutive light flashes. *FEBS Letters* **101,** 201–206.

von Caemmerer S. (2000) *Biochemical Models of Leaf Photosynthesis*. CSIRO Publishing, Australia.

Chang R. (2000) *Physical Chemistry for the Chemical and Biological Sciences*, pp. 448–449. University Science Books, Sausalito, CA.

Chen Y. (1989) *Kinetic studies of mechanism of ubiquinol: cytochrome c2 oxidoreductase of R. sphaeroides: a steady state approach*. PhD thesis, University of Illinois.

Chitnis P.R. (2001) Photosystem I: function and physiology. *Annual Review of Plant Physiology and Plant Molecular Biology* **52,** 593–636.

Cramer W.A., Soriano G.M., Ponomarev M., Huang D., Zhang Z., Martinez S.Z. & Smith J.L. (1996) Some new structural aspects and old concerning the cytochrome b_6f complex of oxygenic photosynthesis. *Annual Review of Plant Physiology and Plant Molecular Biology* **47,** 477–508.

Crofts A.R. (1985) The mechanism of the ubiquinol: cytochrome c oxidoreductase of mitochondria and of *Rhodopseudomoues sphaeroides*. In *The Enzymes of Biological Membranes* (ed. A.M. Martonosi), pp. 347–482. Plenum Publishers Corp., New York.

Crofts A.R., Guergova-Kuras M., Kuras R., Ugulava N., Li J.Y. & Hong S.J. (2000) Proton-coupled electron transfer at the Q_o site: what type of mechanism can account for the high activation barrier? *Biochimica et Biophysica Acta* **1459,** 456–466.

Crofts A.R. & Yerkes C.T. (1994) A molecular mechanism for qE-quenching. *FEBS Letter* **352,** 265–270.

Cruz J.A., Sacksteder C.A., Kanazawa A. & Kramer D.M. (2001) Contribution of electric field ($\Delta\psi$) to steady-state transthylakoid proton motive force (pmf) *in vitro* and *in vivo*. control of pmf parsing into $\Delta\psi$ and ΔpH by ionic strength. *Biochemistry* **40,** 1226–1237.

Demmig-Adams B. & Adams W.W. (1996) Xanthophyll cycle and light stress in nature: uniform response to excess direct sunlight among higher plant species. *Planta* **198,** 460–470.

Ernstsen J., Woodrow I.E. & Mott K.A. (1999) Effects of growth-light quantity, growth-light quality and CO_2 concentration on Rubisco deactivation during low PFD or darkness. *Photosynthesis Research* **61,** 65–75.

Farquhar G.D., Von Caemmerer S. & Berry J.A. (1980) A biochemical model of photosynthetic CO_2 assimilation in leaves of C₃ species. *Planta* **149,** 78–90.

Fernandez-Velasco J.G., Jamshidi A., Gong X.S., Zhou J. & Ueng R.Y. (2001) Photosynthetic electron transfer through the cytochrome b_6f complex can bypass cytochrome f. *Journal of Biological Chemistry* **276,** 30598–30607.

Flores S., Graan T. & Ort D.R. (1983) Measurement of the permeability of the chloroplast thylakoid membrane to amine buffers. *Photobiochemistry and Photobiophysics* **6,** 293–304.

Fridlyand L.E. & Scheibe R. (1999) Controlled distribution of electrons between acceptors in chloroplasts: a theoretical consideration. *Biochimica et Biophysica Acta* **1413**, 31–42.

Frommolt R., Goss R. & Wilhelm C. (2001) The de-epoxidase and epoxidase reactions of *Mantoniella squamata* (Prasinophyceae) exhibit different substrate-specific reaction kinetics compared to spinach. *Planta* **213**, 446–456.

Furbank R.T., von Caemmerer S., Sheehy J. & Edwards G.E. (2009) C4 rice: a challenge for plant phenomics. *Functional Plant Biology* **36**, 845–856.

Gilmore A.M. (1997) Mechanistic aspects of xanthophyll cycle-dependent photoprotection in higher plant chloroplasts and leaves. *Physiologia Plantarum* **99**, 197–209.

Govindjee (1995) Sixty-three years since Kautsky: chlorophyll a fluorescence. *Australian Journal of Plant Physiology* **22**, 131–160.

Gross L.J., Kirschbaum U. & Pearcy R.W. (1991) A dynamic model of photosynthesis in varying light taking account of stomatal conductance, C3-cycle intermediates, photorespiration and Rubisco activation. *Plant, Cell & Environment* **14**, 881–893.

Hahn B. (1984) A mathematical model of leaf Calvin cycle. *Annals of Botany* **54**, 325–339.

Hahn B. (1991) Photosynthesis and photosrespiration. Modeling the essentials. *Journal of Theoretical Biology* **151**, 123–139.

Harley P.C. & Sharkey T.D. (1991) An improved model of C3 photosynthesis at high CO_2: reversed O_2 sensitivity explained by lack of glycerate reentry into the chloroplast. *Photosynthesis Research* **27**, 169–178.

Harley P.C., Thomas R.B., Freynolds J.F. & Strain B.R. (1992) Modelling photosynthesis of cotton grown in elevated CO_2. *Plant Cell and. Environment* **15**, 271–282.

Hong S.J., Ugulava N., Guergova-Kuras M. & Crofts A.R. (1999) The energy landscape for ubihydroquinone oxidation at the Q_o site of the bc_1 complex in *Rhodobacter sphaeroides*. *Journal of Biological Chemistry* **274**, 33931–33944.

Hong S.S. & Xu D.Q. (1999) Light-induced increase in initial chlorophyll fluorescence Fo level and the reversible inactivation of PSII reaction centers in soybean leaves. *Photosynthesis Research* **61**, 269–280.

Horton P., Ruban A.V. & Walters R.G. (1996) Regulation of light harvesting in green plants. *Annual Review of Plant Physiology and Plant Molecular Biology* **47**, 655–684.

Hutchison R.S., Groom Q. & Ort D.R. (2000) Differential effects of chilling-induced photooxidation on the redox regulation of photosynthetic enzymes. *Biochemistry* **39**, 6679–6688.

Joliot P. & Joliot A. (2002) Cyclic electron transfer in plant leaf. *Proceedings of the National Academy of Sciences of the United States of America* **99**, 10209–10214.

Junge W., Auslander W., Mcgeer A.J. & Runge T. (1979) The buffering capacity of the internal phase of thylakoids and the magnitude of the pH changes inside under flashing light. *Biochimica et Biophysica Acta* **546**, 121–141.

Junge W. & Mclaughlin S. (1987) The role of fixed and mobile buffers in the kinetics of proton movement. *Biochimica et Biophysica Acta* **890**, 1–5.

Keirns J.J. & Wang J.H. (1972) Studies on nicotinamide adenine dinucleotide phosphate reductase of spinach chloroplasts. *Journal of Biological Chemistry* **247**, 7374–7382.

Knaff D.B. (1996) Ferredoxin and ferrodxin-dependent enzymes. In *Oxygenic Photosynthesis: The Light Reactions* (eds D. Ort & C.E. Yocum), pp. 10034–10039. The Netherlands, Kluwer.

Kramer D.M., Dimarco G. & Loreto F. (1995) Contribution of plastoquinone quenching to saturation pulse-induced rise of chlorophyll fluorescence in leaves. In *Photosynthesis from Light to the Biosphere*, Vol. **1**. (ed. P. Mathis), pp. 147–150. Kluwer Academic Publishers, Dordrecht.

Kramer D.M., Sacksteder C.A. & Cruz J.A. (1999) How acidic is the lumen? *Photosynthesis Research* **60**, 151–163.

Kramer D.M., Cruz J.A. & Kanazawa A. (2003) Balancing the central roles of the thylakoid proton gradient. *Trends in Plant Science* **8**, 27–32.

Laisk A. (1993) Mathematical modeling of free-pool and channeled electron-transport in photosynthesis – evidence for a functional supercomplex around photosystem I. *Proceedings of the Royal Society of London (B)* **251**, 243–251.

Laisk A. & Edwards G.E. (2000) A mathematical model of C-4 photosynthesis: the mechanism of concentrating CO_2 in NADP-malic enzyme type species. *Photosynthesis Research* **66**, 199–224.

Laisk A., Eichelmann H., Oja V., Eatherall A. & Walker D.A. (1989a) A mathematical model of the carbon metabolism in photosynthesis. Difficulties in explaining oscillations by fructose 2,6-bisphosphate regulation. *Proceedings of the Royal Society of London B* **237**, 389–415.

Laisk A., Oja V., Kiirats O., Raschke K. & Heber U. (1989b) The state of the photosynthetic apparatus in leaves as analyzed by rapid gas exchange and optical methods – the pH of the chloroplast stroma and activation of enzymes in vivo. *Planta* **177**, 350–358.

Laisk A., Oja V., Walker D. & Heber U. (1992) Oscillations in photosynthesis and reduction of photosystem-1 acceptor side in sunflower leaves – functional cytochrome b_6/f-photosystem 1 ferredoxin-NADP reductase super-complexes. *Photosynthetica* **27**, 465–479.

Laisk A., Oja V., Rasulov B., Eichelmann H. & Sumberg A. (1997) Quantum yield and rate constants of photochemical and nonphotochemical excitation quenching. *Plant Physiology* **115**, 803–815.

Laisk A., Eichelmann H. & Oja V. (2006) C-3 photosynthesis in silico. *Photosynthesis Research* **90**, 45–66.

Laisk A. & Walker D.A. (1986) Control of phosphate turnover as a rate-limiting factor and possible cause of oscillations in photosynthesis: a mathematical model. *Proceedings of Royal Society of London* **227**, 281–302.

Laisk A. & Walker D.A. (1989) A mathematical model of electron transport. Thermodynamics necessity for photosystem II regulation: 'Light stroma'. *Proceedings of Royal Soceity of London (B)* **237**, 417–444.

Lazar D. (2003) Chlorophyll a fluorescence rise induced by high light illumination of dark-adapted plant tissue studied by means of a model of photosystem II and considering photosystem II heterogeneity. *Journal of Theoretical Biology* **220**, 469–503.

Lazar D. & Schansker G. (2009) Models of chlorophyll a fluorescence trantrients. In *Photosynthesis in Silico* (eds A. Laisk, L. Nedbal & Govindjee), pp. 85–123. Springer, Dordrecht, The Netherlands.

Leegood R.C. & Walker D.A. (1981) Photosynthetic induction in wheat protoplasts and chloroplasts. Autocatalysis and light activation of enzymes. *Plant, Cell & Environment* **4**, 59–66.

Lelong C., Setif P., Lagoutte B. & Bottin H. (1994) Identification of the amino acids involved in the functional interaction between photosystem I and ferredoxin from *Synechocystis* sp pcc 6803 by chemical cross-linking. *Journal of Biological Chemistry* **269**, 10034–10039.

Liebermeister W. & Klipp E. (2006) Bring metabolic networks to life: convenience rate law and thermodynamic constraints. *Theoretical Biology and Medical Modelling* **3**, 41. doi: 10.1186/1742-4682-3-41.

Long S.P. & Ort D.R. (2010) More than taking the heat: crops and global change. *Current Opinion in Plant Biology* **13**, 241–248.

Long S.P., Humphries S.W. & Falkowski P.G. (1994) Photoinhibition of photosynthesis in nature. *Annual Review of Plant Physiology and Plant Molecular Biology* **45**, 633–662.

Long S.P., Ainsworth E.A., Rogers A. & Ort D.R. (2004) Rising atmospheric carbon dioxide: plants FACE their future. *Annual Review of Plant Biology* **55**, 591–628.

Long S.P., Zhu X.G., Naidu S.L. & Ort D.R. (2006) Can improvement in photosynthesis increase crop yields? *Plant, Cell & Environment* **29**, 315–330.

Martin W., Scheibe R. & Schnarrenberger C. (2000) The Calvin cycle and its regulation. In *Advances in Photosynthesis*, Vol. **9**. (eds R.C. Leegood, T.D. Sharkey & S. von Caemmerer), pp. 9–51. Kluwer Academic Publishers, Dordrecht.

Mate C.J., von Caemmerer S., Evans J.R., Hudson G.S. & Andrews T.J. (1996) The relationship between CO_2-assimilation rate, Rubisco carbamylation and Rubisco activase content in activase-deficient transgenic tobacco suggests a simple model of activase action. *Planta* **198**, 604–613.

Mott K.A. & Woodrow I.E. (2000) Modelling the role of Rubisco activase in limiting non-steady-state photosynthesis. *Journal of Experimental Botany* **51**, 399–406.

Nishio J.N. & Whitmarsh J. (1993) Dissipation of the proton electrochemical potential in intact chloroplasts (II. The pH gradient monitored by cytochrome f reduction kinetics). *Plant Physiology* **101**, 89–96.

Niyogi K.K. (1999) Photoprotection revisited: genetic and molecular approaches. *Annual Review of Plant Physiology and Plant Molecular Biology* **50**, 333–359.

Oja V., Savchenko G., Jakob B. & Heber U. (1999) pH and buffer capacities of apoplastic and cytoplasmic cell compartments in leaves. *Planta* **209**, 239–249.

Ort D.R. (2001) When there is too much light. *Plant Physiology* **125**, 29–32.

Ort D.R., Grandoni P., Ortiz-Lopez A. & Hangarter R.P. (1990) *Perspective in Biochemical and Genetic Regulation of Photosynthesis*. pp. 159–173. Wiley-Liss, New York.

Ort D.R. & Oxborough K. (1992) In situ regulation of chloroplast coupling factor activity. *Annual Review of Plant Physiology and Plant Molecular Biology* **43**, 269–291.

Papageorgiou G.C. (1975) Chlorophyll fluorescence: an intrinsic probe of photosynthesis. In *Bioenergetics of Photosynthesis* (ed. Govindjee), pp. 319–372. Academic Press, New York.

Parry M.A.J., Reynolds M., Salvucci M.E., Raines C., Andralojc P.J., Zhu X.-G., Price G.D., Condon A.G. & Furbank R.T. (2011) Raising yield potential of wheat. II. Increasing photosynthetic capacity and efficiency. *Journal of Experimental Botany* **62**, 453–467.

Pearcy R.W., Gross L.J. & He D. (1997) An improved dynamic model of photosynthesis for estimation of carbon gain in sunfleck light regimes. *Plant, Cell & Environment* **20**, 411–424.

Pettersson G. & Ryde-Pettersson U. (1988) A mathematical model of the Calvin photosynthesis cycle. *European Journal of Biochemistry* **175**, 661–672.

Poolman M.G., Fell D.A. & Thomas S. (2000) Modelling photosynthesis and its control. *Journal of Experimental Botany* **51**, 319–328.

Poolman M.G., Assmus H.E. & Fell D.A. (2004) Applications of metabolic modelling to plant metabolism. *Journal of Experimental Botany* **55**, 1177–1186.

Portis A.R. (1995) The regulation of Rubisco by Rubisco activase. *Journal of Experimental Botany* **46**, 1285–1291.

Portis A.R. (2003) Rubisco activase – Rubisco's catalytic chaperone. *Photosynthesis Research* **75**, 11–27.

Pottosin I.I. & Schonknecht G. (1996) Ion channel permeable for divalent and monovalent cations in native spinach thylakoid membranes. *Journal of Membrane Biology* **152**, 223–233.

Pyke K.A. (1999) Plastid division and development. *The Plant Cell* **11**, 549–556.

Rovers W. & Giersch C. (1995) Photosynthetic oscillations and the interdependence of photophosphorylation and electron transport as studied by a mathematical model. *BioSystems* **35**, 63–73.

Schroppelmeier G. & Kaiser W.M. (1988) Ion homeostasis in chloroplasts under salinity and mineral deficiency. 1. solute concentrations in leaves and chloroplasts from spinach plants under NaCl or NaNO₃ salinity. *Plant Physiology* **87**, 822–827.

Schurmann P. & Buchanan R. (2001) The structure and function of the ferredoxin/thioredoxin system in photosynthesis. In *Advances in Photosynthesis and Respiration* (eds E.M. Aro & B. Andersson), pp. 331–361. Kluwer Academic Publishers, Dordrecht.

Schurmann P. & Jacquot J.P. (2000) Plant thioredoxin systems revisited. *Annual Review of Plant Physiology and Plant Molecular Biology* **51**, 371–400.

Shampine L.F. & Reichelt M.W. (1997) The MATLAB ODE suite. *SIAM Journal on Scientific Computing* **18**, 1–22.

Shampine L.F., Reichelt M.W. & Kierzenka J.A. (1999) Solving index-I DAEs in MATLAB and simulink. *Siam Review* **41**, 538–552.

Shikanai T. (2007) Cyclic electron transport around photosystem I: genetic approaches. *Annual Review of Plant Biology* **58**, 199–217.

Stirbet A., Govindjee, Strasser B.J. & Strasser R. (1998) Chlorophyll a fluorescence induction in higher plants: modelling and numerical simulation. *Journal of Theoretical Biology* **193**, 131–151.

Taly A., Sebban P., Smith J.C. & Ullmann G.M. (2003) The position of Q(B) in the photosynthetic reaction center depends on pH: a theoretical analysis of the proton uptake upon Q(B) reduction. *Biophysical Journal* **84**, 2090–2098.

Thaler M., Simonis W. & Schonknecht G. (1992) Light-dependent changes of the cytoplasmic H⁺ and Cl⁻ activity in the green alga *Eremosphaera viridis*. *Plant Physiology* **99**, 103–110.

Ugulava N.B. & Crofts A.R. (1998) CD-monitored redox titration of the Rieske Fe-S protein of *Rhodobacter sphaeroides*: pH dependence of the midpoint potential in isolated bc₁ complex and in membranes. *FEBS Letters* **440**, 409–413.

Vollmar M., Schilieper D., Winn M. & Buechner C. (2009) Structure of the C14 roter ring of the proton translocating chloroplast ATP synthase. *Journal of Biological Chemistry* **284**, 18228–18235.

Vredenberg W.J. (1976) Electrostatic interactions and gradients between chloroplast compartments and cytoplasm. In *The Intact Chloroplast* (ed. J. Barber), pp. 53–87. Elsevier/North-Holland Biomedical Press, Amsterdam.

Vredenberg W.J. & Bulychev A.A. (1976) Changes in the electrical potential across the thylakoid membranes of illuminated intact chloroplasts in the presence of membrane-modifying agents. *Plant Science Letters* **7**, 101–107.

Walker D. (1992) Concerning oscillations. *Photosynthesis Research* **34**, 387–395.

Winter H., Robinson D.G. & Heldt H.W. (1994) Subcellular volumes and metabolite concentrations in spinach leaves. *Planta* **193**, 530–535.

Witt H.T. (1979) Energy conversion in the functional membranes of photosynthesis analysis by light pulse and electric pulse methods. *Biochimica et Biophysica Acta* **505**, 355–427.

Woodrow I.E. (1986) Control of the rate of photosynthetic carbon dioxide fixation. *Biochimica et Biophysica Acta* **851**, 181–192.

Wullschleger S.D. (1993) Biochemical limitations to carbon assimilation in C3 plants – a retrospective analysis of the A/Ci curves from 109 species. *Journal of Experimental Botany* **44**, 907–920.

Zhang N. & Portis A.R. (1999) Mechanism of light regulation of Rubisco: a specific role for the larger Rubisco activase isoform involving reductive activation by thioredoxin-f. *Proceedings of the National Academy of Sciences of the United States of America* **96**, 9438–9443.

Zhu X.-G. (2010) Systems-level modeling–A new approach for engineering efficient photosynthetic machinery. *Journal of Biotechnology* **149**, 201–208.

Zhu X.-G., Govindjee, Baker N.R., Desturler E., Ort D.R. & Long S.P. (2005) Chlorophyll a fluorescence induction kinetics in leaves predicted from a model describing each discrete set of excitation energy and electron transfer associated with photosystem II. *Planta* **223**, 114–133.

Zhu X.-G., De Sturler E. & Long S.P. (2007) Optimizing the distribution of resources between enzymes of carbon metabolism can dramatically increase photosynthetic rate: a numerical simulation using an evolutionary algorithm. *Plant Physiology* **145**, 513–526.

Zhu X.-G., Long S.P. & Ort D.R. (2008) What is the maximum efficiency with which photosynthesis can convert solar energy into biomass? *Current Opinion in Biotechnology* **19**, 153–159.

Zhu X.-G., Long S.P. & Ort D.R. (2010) Improving photosynthetic efficiency for greater yield. *Annual Review of Plant Biology* **61**, 235–261.

Zhu X.-G., Song Q.F. & Ort D.R. (2012) Elements of a dynamic systems model of canopy photosynthesis. *Current Opinion in Plant Biology* **15**, 237–244.

SUPPORTING INFORMATION

Additional Supporting Information may be found in the online version of this article:

Appendix S1. List of Abbreviations and their Definitions.
Appendix S2. Tables showing the abbreviations of reaction rates, values of parameters and kinetic constants, initial concentrations of metabolites and compounds used in the model of the *e*-Photosynthesis.
Appendix S3. Equations used in *e*-Photosynthesis.